



Characteristics of Deep Tropical and Subtropical Convection from Nadir-Viewing High-Altitude Airborne Doppler Radar

GERALD M. HEYMSFIELD

NASA Goddard Space Flight Center, Greenbelt, Maryland

LIN TIAN

GEST, University of Maryland, Baltimore County, Baltimore, Maryland

ANDREW J. HEYMSFIELD

National Center for Atmospheric Research, Boulder, Colorado

LIHUA LI

NASA Goddard Space Flight Center, Greenbelt, Maryland

STEPHEN GUIMOND

Department of Meteorology, The Florida State University, Tallahassee, Florida

(Manuscript received 6 March 2009, in final form 18 August 2009)

ABSTRACT

This paper presents observations of deep convection characteristics in the tropics and subtropics that have been classified into four categories: tropical cyclone, oceanic, land, and sea breeze. Vertical velocities in the convection were derived from Doppler radar measurements collected during several NASA field experiments from the nadir-viewing high-altitude ER-2 Doppler radar (EDOP). Emphasis is placed on the vertical structure of the convection from the surface to cloud top (sometimes reaching 18-km altitude). This unique look at convection is not possible from other approaches such as ground-based or lower-altitude airborne scanning radars. The vertical motions from the radar measurements are derived using new relationships between radar reflectivity and hydrometeor fall speed. Various convective properties, such as the peak updraft and downdraft velocities and their corresponding altitude, heights of reflectivity levels, and widths of reflectivity cores, are estimated. The most significant findings are the following: 1) strong updrafts that mostly exceed 15 m s^{-1} , with a few exceeding 30 m s^{-1} , are found in all the deep convection cases, whether over land or ocean; 2) peak updrafts were almost always above the 10-km level and, in the case of tropical cyclones, were closer to the 12-km level; and 3) land-based and sea-breeze convection had higher reflectivities and wider convective cores than oceanic and tropical cyclone convection. In addition, the high-resolution EDOP data were used to examine the connection between reflectivity and vertical velocity, for which only weak linear relationships were found. The results are discussed in terms of dynamical and microphysical implications for numerical models and future remote sensors.

1. Introduction

Measurements of updraft characteristics are important for understanding fundamental kinematic and microphysical processes in deep convection. These measurements

are often difficult to obtain from in situ observations because of the transient nature of updrafts and the safety concerns arising from aircraft penetrating convective cores. Consequently, there have been relatively few comparisons between numerically simulated and measured vertical motions through the full depth of deep convective updrafts to evaluate model accuracy (e.g., Lang et al. 2007). Emphasis in recent years on global estimates of tropical latent heating from radar and microwave

Corresponding author address: Gerald M. Heymsfield, Goddard Space Flight Center, Code 613.1, Greenbelt, MD 20771.
E-mail: gerald.heymsfield@nasa.gov

radiometric measurements on the Tropical Rain Measuring Mission (TRMM; Simpson et al. 1996) requires improved knowledge of the vertical motions in precipitation regions since this quantity is not measured. Deep convection distributes heat and moisture in the vertical and is therefore of crucial importance in understanding the dynamics of tropical (and subtropical) regions.

There have been numerous studies of tropical and subtropical convection using aircraft in situ measurements of updrafts (e.g., LeMone and Zipser 1980; Jorgensen and LeMone 1989; Anderson et al. 2005). Many biases in the intensity of convection have often been related to the field experiment, cloud penetration safety issues, the specific aircraft used for the studies, and the type of instrumentation (i.e., in situ or radar). In the convective cells studied by LeMone and Zipser (1980) from the Global Atmospheric Research Program (GARP) Atlantic Tropical Experiment (GATE), updrafts had peak values of $\sim 6 \text{ m s}^{-1}$ that are biased low since the aircraft generally flew below the freezing level. In hurricanes, Jorgensen et al. (1985), using the National Oceanic and Atmospheric Administration (NOAA) WP-3D aircraft (generally confined to altitudes below 6–8 km and biased toward the eyewall regions of intense hurricanes), found that the strongest 10% of updrafts and downdrafts in hurricanes had averages of 4.2 and 2.6 m s^{-1} , respectively, and peak updrafts of $\sim 8 \text{ m s}^{-1}$. Anderson et al. (2005) examined updrafts in tropical convective storms using measurements from the higher-altitude Citation jet aircraft. They examined similarities between tropical oceanic and land cases from TRMM Large-Scale Biosphere–Atmosphere Experiment in Amazonia (LBA) and the Kwajalein Experiment (KWAJEX). Unlike earlier studies that used flight level data, Black et al. (1996) used radial velocities from the NOAA WP-3D tail Doppler radar and reported supercell-like structure in Hurricane Emily (1987) with updrafts and downdrafts as strong as 24 and 19 m s^{-1} , respectively. They found that in the eyewall region, 5% of the vertical motions were $>5 \text{ m s}^{-1}$.

There have been numerous ground-based profiler and multiple Doppler measurements of convection in the tropics and subtropics but fewer measurements over the oceans that have been derived from either in situ or airborne Doppler radar measurements. May and Rajopadhyaya (1999) studied deep convection near Darwin, Australia, using profiler data. They found that updrafts tended to increase with height, with peak values greater than 15 m s^{-1} near the top of their observations (~ 11 -km altitude) and suggested that the peak was reached at a higher altitude. Their study examined three types of convection within the Darwin region that had drastically

different characteristics. One would expect that environmental conditions, which are often a function of geographic location and season, would greatly affect the updraft characteristics in deep convection, leading to a variety of characteristics. The convective storm environment deduced from soundings [e.g., convective available potential energy (CAPE) and vertical wind shear] and low-level forcing can be drastically different, leading to different attributes of convection (e.g., Lucas et al. 1994a; Johnson et al. 2005; May and Rajopadhyaya 1999).

Recent attention has focused on hot towers and vortical hot towers in tropical cyclones since they may have important implications for tropical cyclone intensification, as shown by both theoretical (e.g., Montgomery et al. 2006) and observational (e.g., Simpson et al. 1998; Heymsfield et al. 2001, 2006; Guimond et al. 2010) studies. Observations of hot towers from high-resolution radar measurements (Simpson et al. 1998; Heymsfield et al. 2001, 2006; Halverson et al. 2007; Houze et al. 2009) have shown that hot towers can be very intense, extending to 17- or 18-km altitude with strong updrafts and high reflectivities aloft. In light of this recent work, we are interested in how tropical cyclone hot towers compare with more ordinary intense convection. Improved understanding of hot towers and their role in hurricane intensification will require finer spatial and temporal observational knowledge of their kinematic and microphysical characteristics. The first-order measurement of intense convection linked to these processes is the strength of the vertical motions, which is the emphasis of this paper.

Satellite measurements have been used to define general characteristics of tropical convection. Zipser et al. (2006) studied the most intense thunderstorms within the coverage of TRMM (35°S to 35°N latitude), focusing on four parameters of intense convective storms: three-dimensional radar reflectivity, lightning, passive microwave, and visible/infrared channels. The TRMM satellite does not have Doppler radar measurements so it cannot directly provide information on vertical motions. Zipser et al. (2006) define “intense” storms using the available TRMM measurements as proxies for convective intensity. Common definitions of intense storms from the National Weather Service definition and from ground-based radar measurements include updrafts $>25 \text{ m s}^{-1}$, hail $>1.9 \text{ cm}$ in diameter, or the presence of a tornado (Zipser et al. 2006), and strong wind gusts. The TRMM proxies used by Zipser et al. (2006), Cecil et al. (2005), Nesbitt et al. (2000), and others equate increased storm intensity with 1) increasing height of the 40-dBZ echo above 10-km altitude, 2) decreasing brightness temperatures at 37 and 85 GHz, and 3) greater lightning flash rates in the precipitation

feature. The common property governing all of these proxies is the strength of the vertical motions; thus, there is a need to better understand the relationship between microphysical and kinematic processes in deep convection. Both TRMM and the future Global Precipitation Mission (GPM) use radar reflectivity and radiometer measurements along with cloud models to deduce latent heating. Knowledge of vertical winds can be extremely useful in providing higher-accuracy computations of latent heat through either model improvement or direct use of the observations, such as high-altitude airborne Doppler radar measurements.

Deep convection plays a key role in transport and mixing in the tropical tropopause layer (14–18-km altitude; e.g., Sherwood and Dessler 2000). Extensive upper troposphere cirrus layers in the tropics are often generated by ice mass from deep convective updrafts. The amount of cirrus produced is a complex function of vertical motions and microphysics. Liu and Zipser (2005) suggested that the more intense the convection, the closer the radar echo top is to the infrared (IR) top derived from infrared radiation, indicating a larger potential for mass exchange in the tropical tropopause layer. It is well known that there is a general relationship between updraft strength and the amount of cloud-top overshoot into the tropopause (e.g., Heymsfield et al. 1991; Adler and Mack 1986). Adler and Mack (1986), through modeling of midlatitude severe storms, showed that overshooting cloud parcels that are strongly negatively buoyant will mix with the lower stratospheric environment and eventually subside. Deep convective updraft properties in this higher-altitude region have not been sampled adequately. In addition, downdrafts at all altitudes (particularly upper levels) have not been measured extensively and their documentation in the literature is sparse. Heymsfield and Schotz (1985) found strong ($>10 \text{ m s}^{-1}$) upper-level downdrafts from ground-based Doppler analyses as a result of convergence produced by two adjacent storm outflows. Sun et al. (1994) suggested that upper-level downdrafts can be produced by vertical pressure gradient forces. Thermally buoyant downdrafts were also observed with aircraft (Jorgensen and LeMone 1989). May and Rajopadhyaya (1999) have discussed their profiler data in terms of the above complex mechanisms and concluded that the upper-level downdrafts may in part be due to pressure perturbations induced by strong updrafts.

Early theoretical studies on convective updrafts derived from the vertical equation of motion and the thermodynamic equation in which parcels undergo adiabatic ascent and buoyancy, entrainment, and hydrometeor drag are important factors (e.g., Stommel 1947; Simpson and Wiggert 1969). These models provide in-

sights on the basic physics of convection but are often too simplistic to account for all the complex processes. Lucas et al. (1994b) theorized that updraft width and strength are correlated because mixing and entrainment will, in general, reduce the buoyancy of air parcels. There is still debate over the amount of entrainment in tropical convection and whether tropical oceanic convection is diluted (e.g., Zipser 2003). These observations provide motivation to learn more about updraft characteristics in tropical convection and their variations with height.

In this paper, we utilize high-resolution airborne observations from the downward looking National Aeronautics and Space Administration (NASA) ER-2 Doppler radar (EDOP) to examine vertical motion characteristics during multiple field campaigns dealing with tropical and subtropical deep convection, including hurricanes. Previous observations have stimulated our interest in gathering further statistics about hurricanes versus mesoscale convective system (MCS) hot towers, especially at higher altitudes, where data are scarce to nonexistent.

Section 2 will describe the cases sampled and the methodology both for estimation of vertical velocities and for deriving statistical information from the data. Section 3 presents characteristics of the updrafts to learn more about the regional variation of reflectivity heights and vertical velocity as well as the relationship between peak updraft speeds and reflectivity contour levels. These observational details are important because they have implications for understanding convective dynamics including mass fluxes and latent heating. The statistics presented in section 3 will be compared with previous satellite-based and aircraft-based convection measurements (e.g., Black et al. 1996). Another important aspect of the observations shown in this paper is the ability to provide safety information for instrumented aircraft and unattended aircraft systems (UAS) since these aircraft are being considered for overpasses of hurricanes that contain deep convection. We attempt to describe the relation between reflectivity height contours and vertical velocity since satellite radar measurements such as TRMM only acquire reflectivity measurements and vertical velocity is crucial for latent heating estimates. Section 4 will discuss implications of the observational findings. Finally, a summary of our findings, together with general conclusions, is presented in section 5.

2. Convection cases and analysis methodology

a. EDOP measurements

The NASA ER-2 Doppler Radar flying on the high-altitude ($\sim 20 \text{ km}$) ER-2 aircraft is the primary instrument used for this study. EDOP is an X-band (9.6 GHz)

Doppler radar with dual 3° beams and two antennas, one of which is fixed at nadir while the other is 30° forward of nadir (Heymsfield et al. 1996). Processed reflectivity and Doppler velocity are obtained every 0.5 s, which corresponds to approximately 100 m of aircraft translation (aircraft ground speed $\sim 200\text{--}210\text{ m s}^{-1}$). This configuration oversamples typical convective cores but is implemented to allow for better aircraft motion corrections to the Doppler velocities. The footprint of the nadir beam is $\sim 1.1\text{ km}$ (0.55 km) at the surface (10-km altitude), so the effective resolvability is approximately a few hundred meters at 10-km altitude and 0.5 km near the surface. The profiled Doppler velocities and reflectivities were obtained at 37.5 m (75 m prior to 1997) intervals in the vertical. The Nyquist velocity is $\sim 34\text{ m s}^{-1}$ so unfolding was not required. The main editing on raw Doppler velocities was removing noisy data by using a power threshold and corrections for aircraft motions. The aircraft motions are removed from the raw Doppler velocities using the ER-2 inertial navigation system (INS) and the antenna tilt angles. Details of these procedures can be found in Heymsfield et al. (1999, 2001, 2006).

The reflectivity data have been calibrated to within about 1 dBZ by internal and external calibrations and checked against the ocean surface return. The minimum detectable reflectivity of EDOP varied between datasets (mainly by year): 0 dBZ at 10-km range (10-km altitude) during 1995–97 and -10 dBZ at 10-km range after 1997. Reflectivities were corrected for attenuation using the “hybrid” surface reference approach (Iguchi and Meneghini 1994). Reflectivity without this correction would result in lower values in the rain region where most of the attenuation occurs. The attenuation correction is of lower accuracy over land since the background (non-precipitating) surface reflectivity returns are more difficult to estimate (Tian et al. 2002); also, the earliest datasets from 1995 had a lower accuracy surface estimate due to lower-resolution vertical sampling.

The Doppler velocities with aircraft motion removed are vertical hydrometeor motions (v_h) from which the vertical air motion $w = v_h + v_t$ can be obtained with a hydrometeor fall speed (v_f) assumption based on the reflectivity. The estimates used for v_t are described in more detail in the appendix. Once the fall speeds are estimated and added to the hydrometeor motions, a nine-point median filter is used to remove spurious values (spikes) from the data without altering the widths of features. The main filtering on the data is by the radar beam itself, whose width increases from 0 km near the plane to $\sim 500\text{ m}$ at 10-km altitude to $\sim 1\text{ km}$ near the surface; data oversampling by a factor of 5 will result in a resolution less than these height-dependent beam widths. The EDOP antenna side lobes are 56 dB (two-

way) down from the main antenna lobe, so these will not appreciably broaden the width of the measurements. Earlier work by LeMone and Zipser (1980), Anderson et al. (2005), and others defined their updrafts with vertical velocity thresholds over 0.5 km along the flight line, so these differences should be noted in subsequent discussion. LeMone et al. (1994) examined the effects of filtering on their vertical velocity data to identify updrafts and downdrafts and their conclusions do not seem to recommend filtering.

b. Convection cases

Table 1 lists various NASA field campaigns from 1995 to 2005 during which the EDOP radar on the ER-2 flew above strong convection. These campaigns cover a variety of oceanic and land regions. Further information on the campaigns can be found in the references provided in Table 1. The only nonmajor campaign in Table 1 was the Houston Precipitation Experiment (HOPEX), conducted primarily for the first EDOP test flights. The EDOP flight lines were examined for strong convective cells, defined by having either 1) a strong updraft ($>10\text{ m s}^{-1}$) over at least a kilometer along the flight track or 2) a 20-dBZ echo extending up to 12-km altitude or greater. The rationale for using either of these parameters is that convection often evolves where updrafts are strongest and reflectivities weakest in the early to mature lifetime, and reflectivities and downdrafts are strongest in the mature and dissipating periods, making it difficult to rely on just one of the parameters. Using both parameters provides an indirect method for handling cell evolution.

Table 2 displays 65 cases of strong to intense convection assembled from different field experiments, providing the approximate center location and time of each cell, the type of convection, and the field campaign. Hot towers are included from five hurricanes, Bonnie (1998), Georges (1998), Humberto (2001), Dennis (2005), and Emily (2005), and two tropical storms, Chantal (2001) and Gert (2005). Some of these storms have already been analyzed in papers such as Heymsfield et al. (2001, 2006), Geerts et al. (2000), Halverson et al. (2007), and Guimond et al. (2010). Some of the land-based and oceanic cases have been reported in Tian et al. (2002).

Figure 1 shows the locations of the convective events sampled by EDOP sorted into four categories: land (Florida, Brazil, Gulf Coast, Central America), oceanic (Caribbean, eastern Pacific, Gulf of Mexico), tropical cyclone (Atlantic and eastern Pacific), and sea breeze (Florida). The sea-breeze cases were separated from land-based convection since they are likely initiated by different mechanisms than pure oceanic or land-based convection; they were very close to the coastline (within

TABLE 1. Field campaigns with overflights by EDOP.

Field Campaign	Acronym	Date	Objectives	Reference
Houston Precipitation Experiment	HOPEX	Jan 1995	EDOP test flights	Heymsfield et al. (1999)
Convection and Moisture Experiment-2	CAMEX-2	Aug–Sep 1995	Convection, water vapor	Heymsfield et al. (1996)
Convection and Moisture Experiment-3	CAMEX-3	Jul–Sep 1998	Convection, tropical storms, TRMM validation	Kakar et al. (2006)
TRMM Large-Scale Biosphere–Atmosphere Experiment	TRMM-LBA	Jan–Feb 1999	Precipitation systems, convection, TRMM validation	http://disc.sci.gsfc.nasa.gov/fieldexp/TRMM_FE/lba/
Convection and Moisture Experiment-4	CAMEX-4	Aug–Sep 2001	Convection, tropical storms, TRMM validation	Kakar et al. (2006)
Cirrus Regional Study of Tropical Anvils and Cirrus Layers–Florida Area Cirrus Experiment	CRYSTAL-FACE	Jul 2002	Tropical cirrus, aerosols, chemistry, EOS validation	Jensen et al. (2004)
Tropical Cloud Systems and Processes	TCSP	Jul 2005	Tropical storms, convection	Halverson et al. (2007)
Tropical Composition, Cloud and Climate Coupling	TC4	Jul 2005	Tropical cirrus, aerosols, chemistry	Starr (2008)

~30 km). The location of each case is shown in both the full-scale map and also in the four zoomed panels; symbols in the zoomed panels correspond to cases in Table 2. The cases represent a wide assortment of convection types in the Northern Hemisphere warm season with the exception of the Louisiana cases, which were flown during winter. On average, the freezing level is at 4.5–5-km altitude for the warm season and around 3.7-km altitude for the cold season in Louisiana. Diurnal variations are not considered since the aircraft overpass times vary widely because of both the presence of convection and aircraft safety (landing) issues. This may be an issue in overall generalizations about the data since intense convection often peaks in the afternoon over land with no peak activity over ocean (e.g., Zipser et al. 2006). Another factor worth noting is that satellite studies (e.g., Petersen and Rutledge 2001) show major differences in convective intensity for ocean cases within several hundred kilometers of the coast and those out over the open ocean. Many of the ocean cases studied are near coastal regions.

c. Analysis methodology

As mentioned previously, intense convection in the current study is defined by either a 20-dBZ echo above 12-km altitude or by updrafts with magnitudes $\geq 10 \text{ m s}^{-1}$ at any altitude. There have been many definitions of intense convection as described by Zipser et al. (2006). For example, they defined a strong updraft as having a 40-dBZ echo above 10 km and $>10 \text{ m s}^{-1}$ velocity above 8 km. The rationale for the case selection in this paper is de-

scribed below but was initially based on a subjective appearance of strong, deep convection in the EDOP data with refinement according to the above criteria. It is well known that convection can be comprised of isolated, easily identifiable cells as well as complicated multiple cellular structures in close proximity. In the current study, we do not attempt to separate cells into different stages of development, but we do try to isolate adjacent cells in multicellular situations as much as possible. Convective cells undergo life cycles from growing to mature to dissipating stages. The EDOP cross sections are snapshots during an instant of a convective cell's lifetime. To complicate matters, the life cycle of vertical velocity and precipitation are not always in phase (i.e., updrafts tend to be strongest during early to mature periods of cell development and precipitation and reflectivities are strongest during the mature and dissipating periods).

In addition to the above, there are other aspects of the EDOP cross sections that will affect interpretations. First, flight tracks may not cross the peak of storm cores or updrafts may be tilted causing only certain levels to be captured. Also, strong cross-winds to the ER-2 flight direction from either vertical wind shear or tropical cyclone tangential motions may affect the vertical velocity calculations because of inadequate aircraft motion removal and a crosswind bias (Heymsfield 1989). Finally, the selection of flight legs during field campaigns focused on particular events or on strong convection, so our dataset does not provide a statistical sampling of convection with differing intensities, of diurnal cycle, or seasonal variations. The focus on mean profiles of peak

TABLE 2. Convection cases. Categories of convection are land (L) with 22 cases, tropical cyclone (T) with 13 cases, oceanic (O) with 22 cases, and sea breeze (S) with 8 cases.

ID	Date (yymmdd)	Time (UTC)	Lat (°N)	Lon (°E)	Description	Campaign	Category
A	950106	2046:19	30.43	89.8	Mississippi winter convection	HOPEX	L
B	950106	2057:47	29.38	-90.5	Louisiana winter convection	HOPEX	L
C	950106	2219:16	29.92	-89.3	Louisiana winter convection	HOPEX	L
D	950106	2221:18	29.71	-89.4	Louisiana winter convection	HOPEX	L
E	950826	2133:40	33.26	-79.3	S. Carolina land convection	CAMEX2	L
F	950826	2200:47	34.36	-82.6	S. Carolina land convection	CAMEX2	L
G	950826	2211:35	33.89	-83.8	S. Carolina land convection	CAMEX2	L
H	950828	2208:46	34.67	-73.6	N. Carolina ocean convection	CAMEX2	O
I	950828	2307:59	30.79	-78.1	SC/Georgia ocean convection	CAMEX2	O
J	950828	2309:11	30.93	-78.1	SC/Georgia ocean convection	CAMEX2	O
K	980808	1735:56	27.38	-80.9	Florida land convection	CAMEX3	L
L	980808	1749:34	27.43	-80.9	Florida land convection	CAMEX3	L
M	980815	2228:44	28.27	-81.1	Florida sea-breeze convection	CAMEX3	S
N	980815	2237:48	28.15	-81.1	Florida sea-breeze convection	CAMEX3	S
O	980823	1959:02	24.61	-71.4	Hurricane Bonnie Cat. 3	CAMEX3	T
P	980824	2230:54	26.73	-72.7	Hurricane Bonnie Cat. 3	CAMEX3	T
Q	980905	2220:02	28.74	-82.1	Florida land convection	CAMEX3	L
R	980917	1924:54	27.65	-85.2	Gulf of Mexico convection (FL)	CAMEX3	O
S	980917	1947:17	26.68	-84	Gulf of Mexico convection (FL)	CAMEX3	O
T	980921	1721:04	17.66	-64.5	Hurricane Georges Cat. 2	CAMEX3	T
U	980922	2318:29	18.82	-70.7	Hurricane Georges Cat. 2	CAMEX3	T
V	990125	2221:22	-12.3	-61.9	Brazil Rhondonia convection	LBA	L
W	990125	2243:34	-12.4	-62.1	Brazil Rhondonia convection	LBA	L
X	990125	2309:07	-12.4	-62.1	Brazil Rhondonia convection	LBA	L
Y	990207	1859:24	-10.7	-61.6	Brazil Rhondonia convection	LBA	L
Z	990207	1919:23	-10.7	-61.6	Brazil Rhondonia convection	LBA	L
a	990210	1814:13	-10.7	-61.9	Brazil Rhondonia convection	LBA	L
b	990212	1814:24	-11.3	-61.9	Brazil Rhondonia convection	LBA	L
c	990212	2052:23	-11	-61.2	Brazil Rhondonia convection	LBA	L
d	990221	1842:11	-10.6	-61	Brazil Rhondonia convection	LBA	L
e	010820	2117:20	18.37	-86.5	TS Chantal hot tower	CAMEX4	T
f	010922	1936:04	29.37	-66.7	Hurricane Humberto hot tower	CAMEX4	T
g	010907	1736:47	26.18	-83.6	Gulf of Mexico convection (FL)	CAMEX4	O
h	010919	1758:01	24.71	-81	Key West convection	CAMEX4	S
i	010919	1814:42	24.7	-80.9	Key West convection	CAMEX4	S
j	020707	2026:28	26.44	-82.4	Florida sea-breeze convection	CRYSTAL	S
k	020707	2135:20	25.66	-81.3	Florida sea-breeze convection	CRYSTAL	S
l	020716	1945:40	25.67	-80.6	Florida land convection	CRYSTAL	L
m	020723	2005:56	27.32	-80.4	Florida sea-breeze convection	CRYSTAL	S
n	020728	2047:60	26.27	-81.3	Florida land convection	CRYSTAL	L
o	020728	2155:52	26.4	-81.9	Florida sea-breeze convection	CRYSTAL	S
p	050702	1509:11	15.05	-81	Caribbean Sea convection	TCSP	O
q	050707	0055:37	16.11	-73.2	Hurricane Dennis Cat. 1	TCSP	T
r	050707	0133:00	16.52	-73.3	Hurricane Dennis Cat. 1	TCSP	T
s	050709	1429:56	24.55	-83.5	Hurricane Dennis Cat. 2	TCSP	T
t	050709	1:53:42	24.7	-83.6	Hurricane Dennis Cat. 2	TCSP	T
u	050717	0753:20	17.89	-81.8	Hurricane Emily Cat. 4	TCSP	T
v	050717	0844:20	17.91	-82.1	Hurricane Emily Cat. 4	TCSP	T
w	050720	0640:01	10.59	-86.4	Costa Rica Pacific convection	TCSP	O
x	050723	0842:25	13.12	-84.6	Nicaragua land convection	TCSP	L
y	050723	0919:41	11.29	-82.6	Caribbean Sea convection	TCSP	O
z	050724	0452:05	21.15	-94.3	TS Gert hot tower/Campeche	TCSP	T
1	070808	1617:24	7.92	-83.9	Costa Rica Pacific Ocean	TC4	O
2	070808	1619:8	7.84	-83.8	Costa Rica Pacific Ocean	TC4	O
3	070717	1615:18	5.6	-82	Caribbean Sea	TC4	O
4	070719	1423:46	9.1	-85.4	Costa Rica Pacific Ocean	TC4	O
5	070724	1323:42	6.74	-86.4	Costa Rica Pacific Ocean	TC4	O

TABLE 2. (Continued)

ID	Date (yymmdd)	Time (UTC)	Lat (°N)	Lon (°E)	Description	Campaign	Category
6	070724	1329:46	6.37	-85.9	Costa Rica Pacific Ocean	TC4	O
7	070724	1340:30	5.69	-84.9	Costa Rica Pacific Ocean	TC4	O
8	070724	1329:28	6.38	-85.9	Costa Rica Pacific Ocean	TC4	O
9	070724	1454:50	6.02	-85.7	Costa Rica Pacific Ocean	TC4	O
#	070724	1503:11	6.57	-86.5	Costa Rica Pacific Ocean	TC4	O
*	070725	1503:22	15.92	-82.7	Caribbean Sea	TC4	O
\$	070731	1601:59	9.09	-84.8	Costa Rica Pacific Ocean	TC4	O
%	070731	1635:49	8.96	-84.9	Costa Rica Pacific Ocean	TC4	O

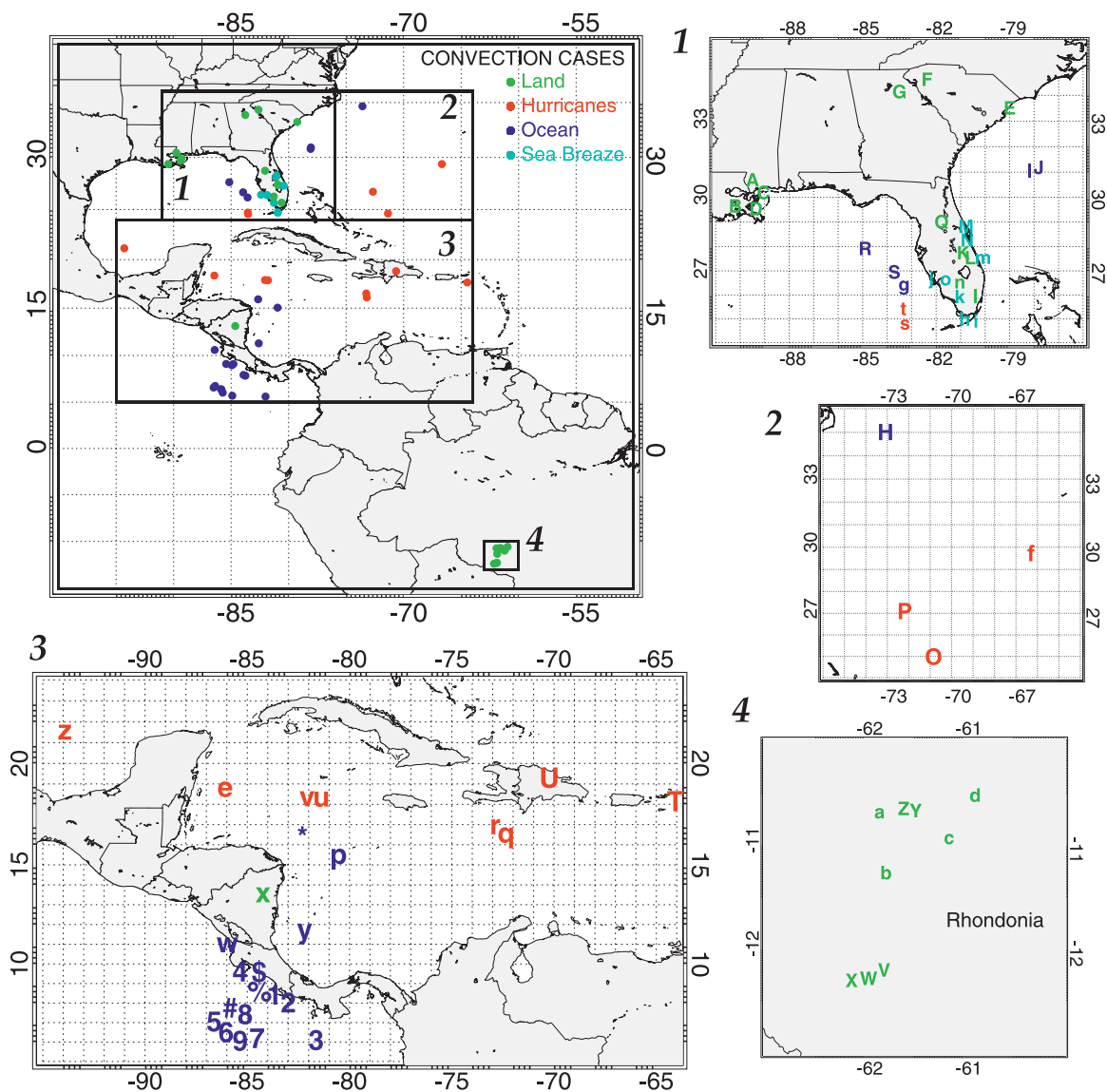


FIG. 1. Map showing locations of all cases from Table 2 (top left) along with four subset regions. Each case is denoted with a symbol provided in Table 2. The convection cases are color coded according to convection type (land, tropical storms, ocean, and sea breeze). Zoomed subset regions 1–4 are shown along with case locations; Rondonia is in Brazil.

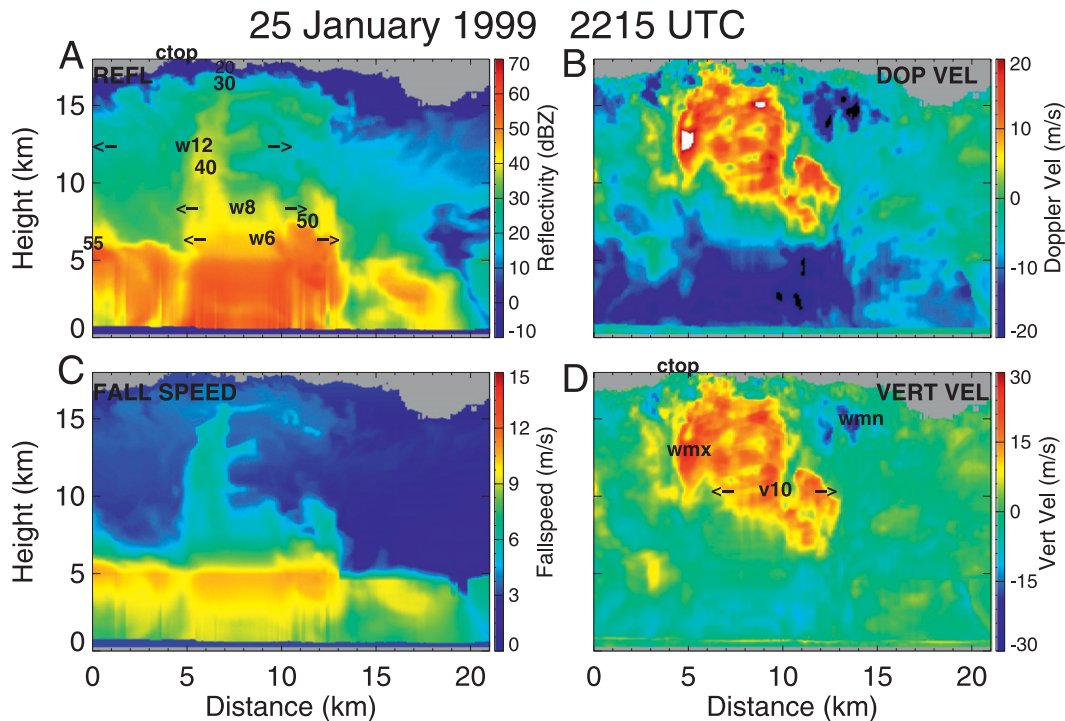


FIG. 2. EDOP color cross sections for convection in Amazonia on 25 Jan 1999 (case V), showing (a) reflectivity, (b) Doppler velocity corrected for aircraft motions, (c) fall speed, and (d) vertical velocity. Locations of quantities derived from the data are also shown on the images in (a) and (d); (a) shows heights of contour levels (20, 30, 40, 50, 55 dBZ), width of 35 dBZ at 6-km altitude (w6), width of 30-dBZ contour at 8-km altitude (w8), and maximum cloud top (CTOP); (d) shows updraft maximum (WMX) and minimum (WMN), CTOP, and width of 5 m s^{-1} updraft bounds at 10-km altitude. Doppler velocities are positive downward. See text for details.

updraft properties in this paper will help reduce some of these sampling uncertainties.

Calculations were performed on cases in Table 2 for various properties of the convection. To simplify the analysis, the EDOP flight lines were zoomed to approximately 10–15 km on either side of the convective core. The appendix provides the computational procedures for calculating vertical velocity, w , from Doppler velocity and assumed hydrometeor fall speeds. The zoomed EDOP time–height sections (Figs. 2–4) show the entire convective region maximum and minimum reflectivity w at each altitude, maximum heights of reflectivity levels (20, 30, 40, and 50 dBZ), magnitude and heights of maximum updrafts and downdrafts, widths of updraft cores, radar-derived cloud-top height, and other properties derived from other ER-2 instruments. Three examples from Table 2 illustrate the above calculations: intense convection in Rhondonia, Brazil, on 25 January 1999 (Fig. 2; case V); Tropical Storm Chantal on 20 August 2001 (Fig. 3; case e); and sea-breeze convection along Florida’s Atlantic coast on 23 July 2002 (Fig. 4; case m). The cases in Table 2 are quite varied; some have strong persistent isolated cells while others are shorter

lived with multicellular structure. We note that altitudes in these and other figures throughout the paper are referenced to the Global Positioning System (GPS) altitude, so they are closer to “above sea level” than “above ground level.” The majority of our cases are near sea level, with a $\sim 550\text{-m}$ surface elevation for the TRMM LBA cases, for example. TRMM measurements studied by Zipser et al. (2006) and others are based on GPS altitudes that are referenced to geoids so we are most consistent with these satellite-based studies. Another point to note is that peak values derived in the radar measurements have been filtered by the radar beam over a broader area than previous aircraft flight-level vertical velocity measurements such as Jorgensen et al. (1985). They showed that when the aircraft did not pass directly through the updraft maximum, it could be underestimated by a factor of 2 for mass fluxes. It is important for the reader to be aware of these differences in subsequent discussion.

Figures 2–4 show reflectivity, Doppler velocity corrected for aircraft motions, fall speed, and w , with derived quantities superimposed on panels (a) and (d). Figure 2 is an intense tower with a cloud top exceeding 17-km

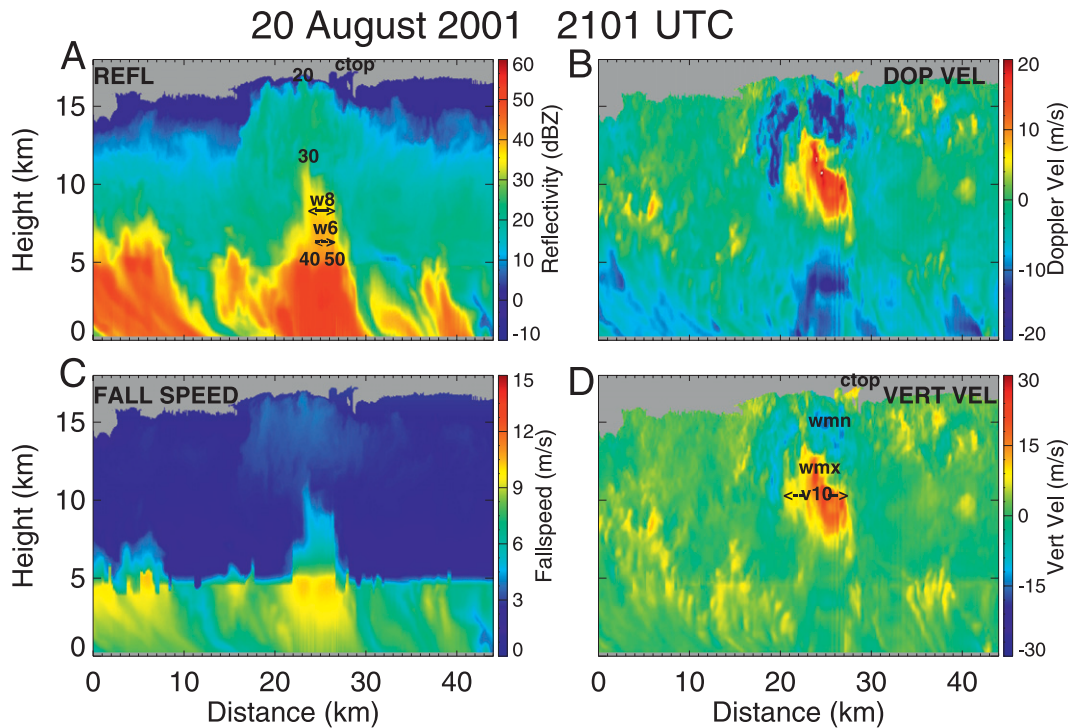


FIG. 3. As in Fig. 2, but for the case on 20 Aug 2001 (Tropical Storm Chantal; case e).

altitude, a 30-dBZ echo at a height of ~ 16 km, 40-dBZ height at ~ 6 km, w_{\max} at ~ 12 -km altitude, and an updraft width defined by updraft region > 5 m s $^{-1}$ at 10-km altitude (v_{10}) of 8–10 km. This tower is among the strongest cases in Table 2 and it is highly attenuated with two-way path-integrated attenuation larger than 40 dBZ (not shown). This amount of attenuation is likely an indicator of small hail since 1-cm hail will attenuate an X-band signal about 7 dB km $^{-1}$ (Battan 1973, p. 81; see his Table 6.5).

Petersen and Rutledge (2001) examined the variations of convective regimes during TRMM-LBA and their plots show that 40-dBZ echoes rarely get above 8-km altitude and that 30-dBZ contours peak around 14 km. They mention that more intense convection occurs during the easterly regime that was present during this case, but their results are still consistent with the heights in Fig. 2.

The Tropical Storm Chantal example in Fig. 3 was previously reported in Heymsfield et al. (2006) and Herman and Heymsfield (2003). The 30-dBZ height is lower than that for the previous case, the updraft width is ~ 5 –6 km, and w_{\max} and w_{\min} again are at an altitude above 10 km. A typical Florida land-based convective storm (Fig. 4) has a much narrower updraft and has mostly multiple cells. It is easy to distinguish two updraft pulses in this cross section. The one on the right has higher reflectivities but the updraft has dissipated, and

a new pulse on the left tower has a strong updraft with a width of only about 2 km. Even though there are large dissimilarities between this case and the two previous cases, the general updraft properties of a number of cases are similar, as will be seen in the next section.

Vertical profiles in Figs. 5 and 6 show the range of values corresponding to the panels in Figs. 2 and 3. The maximum and minimum, median, and ± 2 standard deviation ($\pm 2\sigma$) vertical profiles are plotted for each panel; we have not plotted the full frequency diagram since it was difficult to discern the profile properties. As noted in previous figures, updraft and downdraft maxima are at higher altitudes. Figure 5 indicates an updraft approaching 28 m s $^{-1}$ at ~ 17 -km altitude and a downdraft of 18 m s $^{-1}$ at 16-km altitude. A second updraft peak of ~ 26 m s $^{-1}$ is noted at about 11-km altitude. The maximum reflectivity profile exceeds 60 dBZ near the melting level, drops off to 40 dBZ at 10-km altitude, and remains at ~ 35 dBZ until about 16-km altitude. A slightly weaker updraft and downdraft is present in Fig. 6 for Tropical Storm Chantal, but more notable is the difference in depth of the intense updraft. Strong downdrafts ~ 15 m s $^{-1}$ near cloud top at 15-km altitude have been documented in the literature (Heymsfield and Schotz 1985; Sun et al. 1994), as mentioned earlier. The above two cases clearly show that updrafts are strong through the troposphere, and that peak values are observed at higher altitudes.

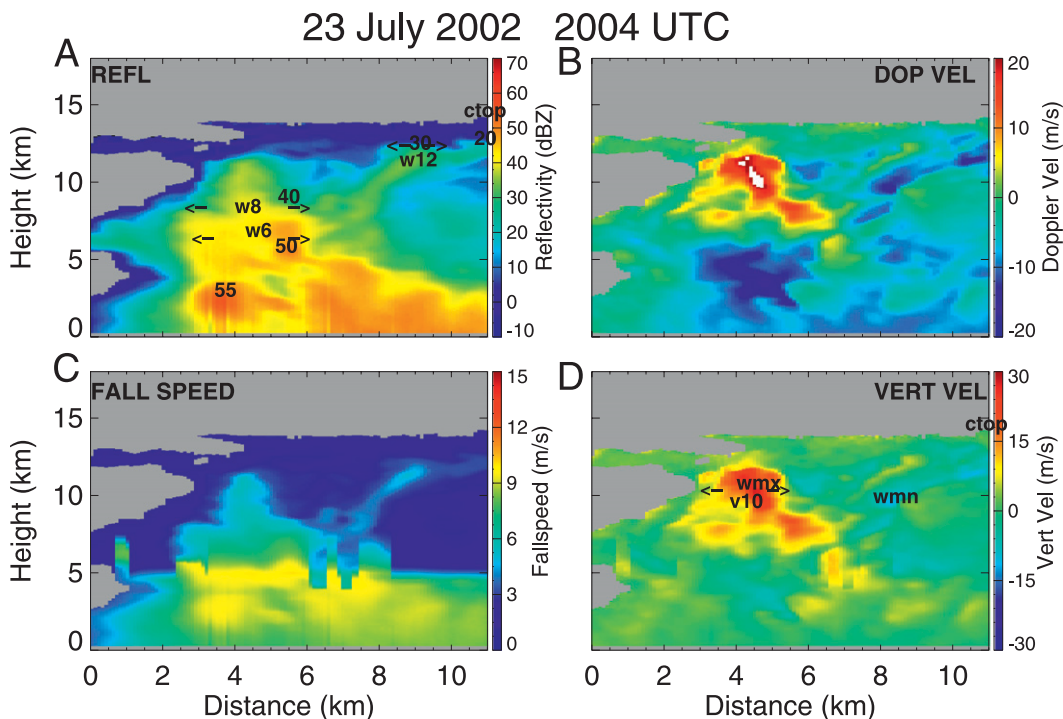


FIG. 4. As in Fig. 2, but for the case on 23 Jul 2002 (thunderstorm over Florida; case m).

3. General characteristics of convective structure

a. General convection features

The plots in the following sections (Figs. 7–10) have been constructed using quantities calculated similar to those in Figs. 2–4. The panels in each plot are divided into the four categories of convection included in Table 2 (tropical cyclone, land, oceanic, and sea breeze), and within each category, the points are identified by location of the data source provided in Table 2. Means are taken within each category. The cases within each category are further sorted so vertical motion maxima increase toward the right. This type of plot allows quick comparison between the diverse set of cases in this study.

1) VERTICAL VELOCITY MAXIMA AND MINIMA (FIG. 7)

The observations clearly show that strong updrafts exist through the troposphere. Peak vertical velocities range from 6 m s^{-1} to greater than 30 m s^{-1} in Fig. 7a. Oceanic and tropical cyclone cases suggest slightly lower peak vertical velocities than land and sea-breeze cases ($2\text{--}5 \text{ m s}^{-1}$ in the mean); sea-breeze cells had among the strongest updrafts. These updraft magnitudes are not surprising and have been observed previously by in situ measurements (Herman and Heymsfield 2003; Jenkins

et al. 2008), but they are somewhat higher than that observed by Anderson et al. (2005; maximum value of $\sim 16 \text{ m s}^{-1}$), presumably because of aircraft safety concerns with stronger cells.

Peak downdrafts (Fig. 7b) are also quite strong, ranging from a few to $\sim 19 \text{ m s}^{-1}$; the land and sea-breeze convection has significantly stronger average peak downdrafts than the oceanic or tropical cyclone convection (~ 17 versus $\sim 11 \text{ m s}^{-1}$ in the mean). While it is clear that strong downdrafts are associated with strong updrafts, there is no correlation between peak updrafts and peak downdrafts for any of the categories. The intensity of both peak updrafts and downdrafts is weaker for the oceanic and tropical storm cases than for the other convection categories. As mentioned earlier, the downdrafts are complex and further understanding of the mechanisms producing these downdrafts will likely require numerical modeling.

Heights of w_{max} (Fig. 7c) occur frequently above 8 km, but they are mainly above 10 km; a few cases have peak updraft below the 8-km level and a few have heights above the 15-km level. The observed vertical motion peak in the upper troposphere is hypothesized to be the result of latent heat release caused by freezing of ice condensate (e.g., Zipser 2003), and/or hydrometeor unloading, which reduces the drag on ascending air parcels. Heights of downdrafts w_{min} (Fig. 7d) are generally in the upper troposphere with some downdrafts

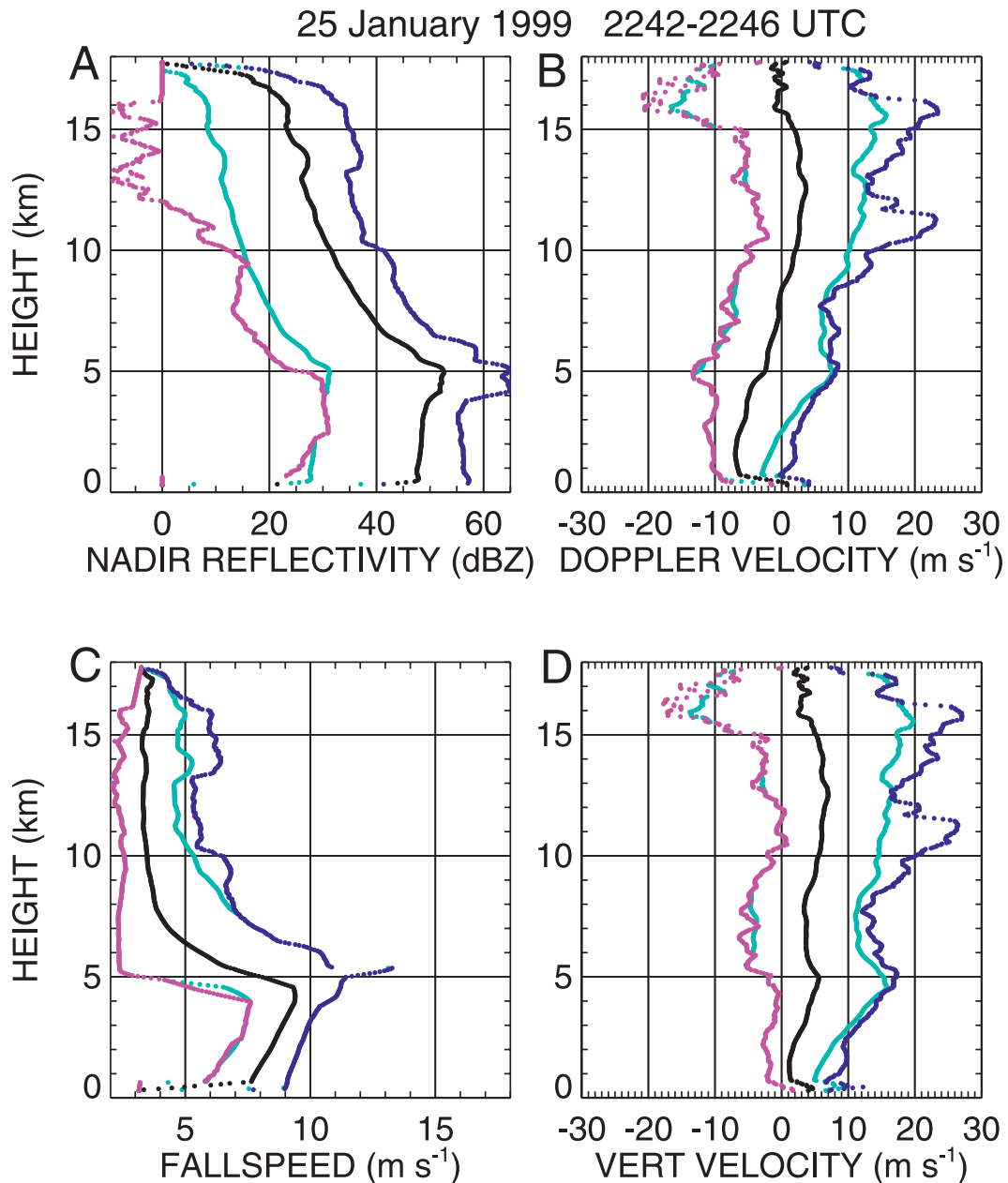


FIG. 5. Profiles of (a) nadir reflectivity, (b) Doppler velocity, (c) fall speed, and (d) vertical velocity for 25 January 1999 corresponding to flight line in Fig. 2. The minimum (purple), maximum (blue), mean (black), and $\pm 2\sigma$ values (turquoise) are shown; the $+2\sigma$ reflectivity curve in (a) is not shown since it exceeds the maximum value.

near cloud top; there are a few cases in each category that have downdraft peak heights in the 5–10-km range. Interestingly, w_{max} heights are 2 km higher in tropical cyclones than other categories, whereas w_{min} heights are 1–2 km lower than other categories. The height of w_{max} is mostly above 10 km for land-based storms (Florida, continental United States, and Louisiana winter). This may be a manifestation of drier midlevel environments for these cases.

2) REFLECTIVITY LEVEL HEIGHT CONTOURS (FIG. 8)

The heights of peak reflectivity of 20, 30, 40, and 50 dBZ range in altitude from ~11 to 18 km, ~5 to 17 km, ~3.5 to 15 km, and 0 to 11 km (0 km indicates that no 50-dBZ reflectivity was detected in the column), respectively. Most of the cases suggest that high reflectivity aloft, such as the 30-dBZ contour level above

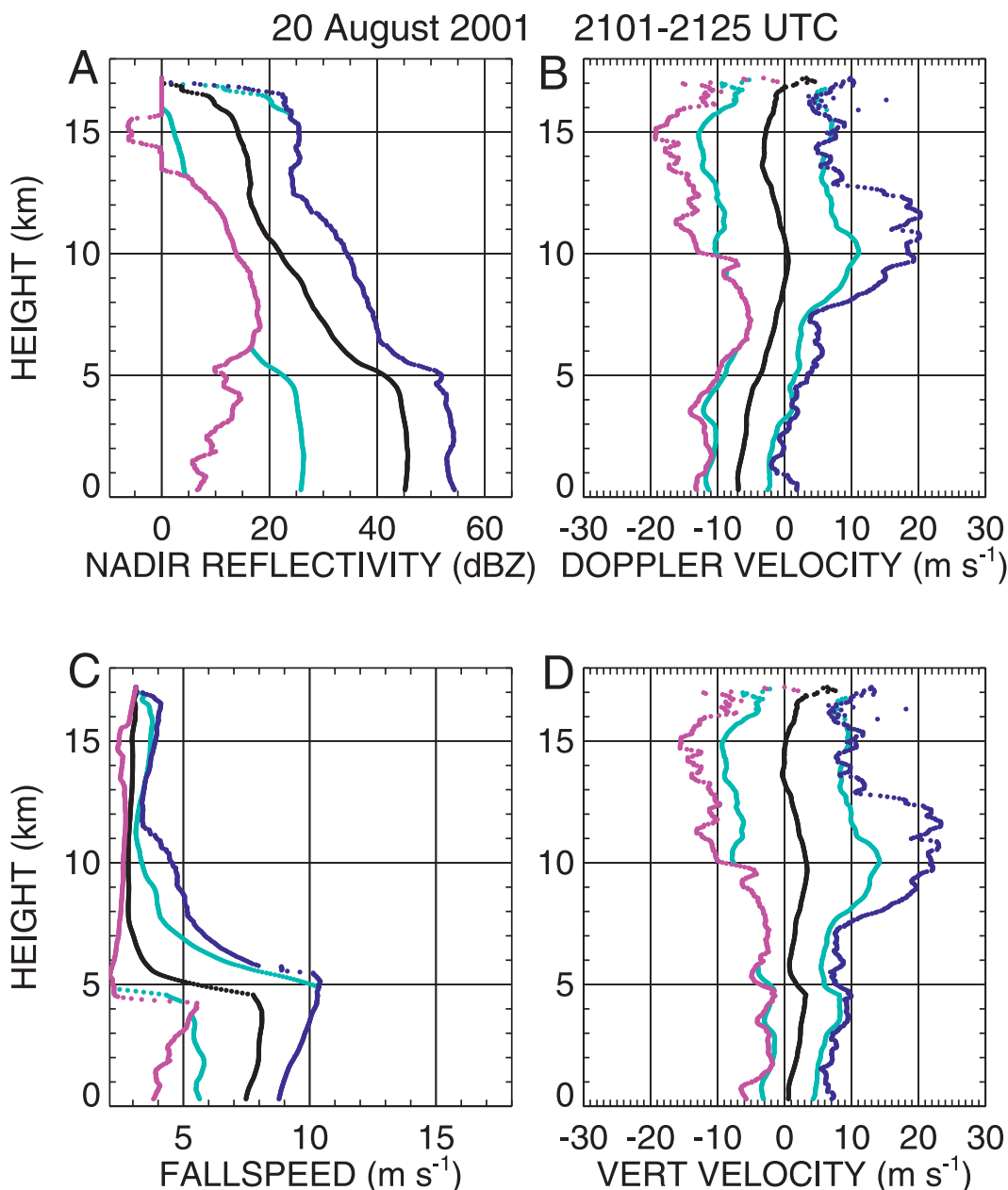


FIG. 6. As in Fig. 5, but for 20 August 2001, corresponding to Fig. 3.

8–10 km, is correlated with strong updrafts in Fig. 7. On the average, the heights for oceanic and tropical cyclone cases are lower by about 0.5 to 1 km than that of the land and sea-breeze categories. Eastern Pacific oceanic storms have lower reflectivities than that of the other oceanic cases. A few hurricane and sea-breeze cases have the highest 40- and 50-dBZ heights. Many 50-dBZ heights (Fig. 8d) are at 5–7-km altitude (0° to -10°C), suggesting that supercooled raindrops are lofted above the freezing level and freeze near the -10°C level. This is consistent with the Stith et al. (2004) results

in which they observed raindrop freezing in the -10° to -20°C level in various convective cells. There is a $\sim 6.5\text{-dB}$ increase in the reflectivity between the ice and water phase because of the increase in the dielectric coefficient (Smith 1984). This results in sharp decreases in reflectivity above the 5–6-km altitude in many of the cases. We will discuss this subject further in section 4.

Three cases were especially strong compared to the others. Sea-breeze cases M and N (15 August 1998) had centimeter-size hail based on ground-based S-band

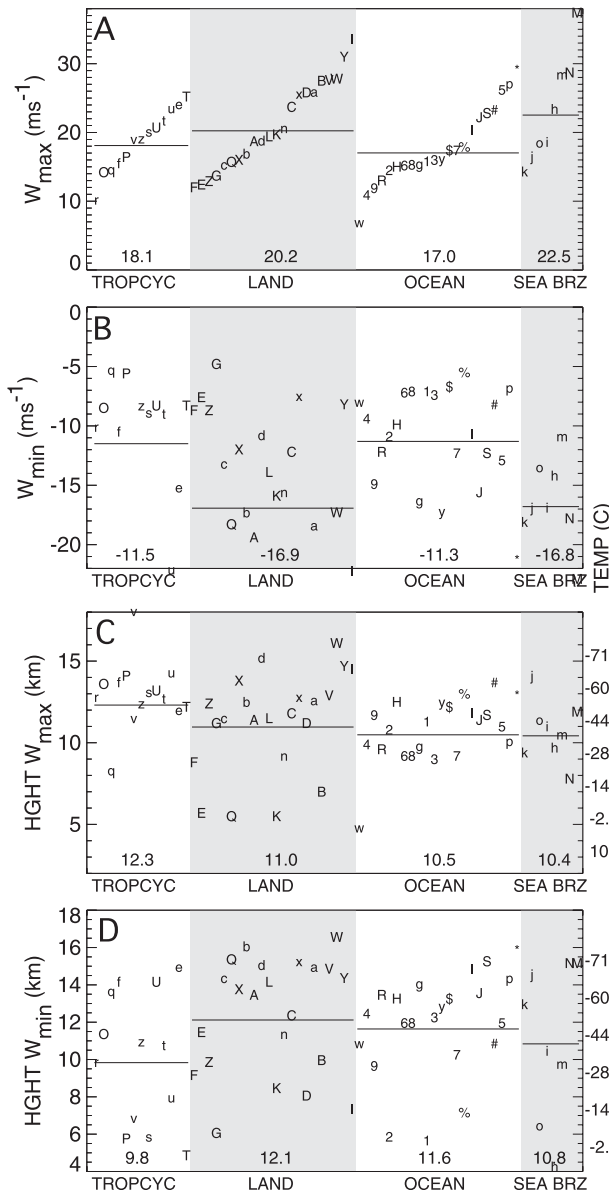


FIG. 7. (a) Updraft maxima, (b) downdraft maxima, (c) height of updraft maxima, and (d) height of downdraft maxima, for all cases. Characters and numbers in figure are referenced to cases in Table 2. Four categories of convection—tropical cyclone, land (shaded), oceanic, and sea breeze (shaded)—are shown within each category; peak updraft increases toward the right. Shaded region highlights land-based and sea-breeze convection cases. Horizontal line provides mean for each category and actual mean is given at bottom of each category. Approximate environment temperature scale is provided on the right for (b)–(d).

polarimetric radar data (Tian et al. 2002). Case u (Hurricane Emily) clearly stands out as well; both storms had 40 dBZ extending up to 14–15-km altitude, which fits among the strongest storms in the Zipser et al. (2006) study. The Brazil cases V and W (25 January

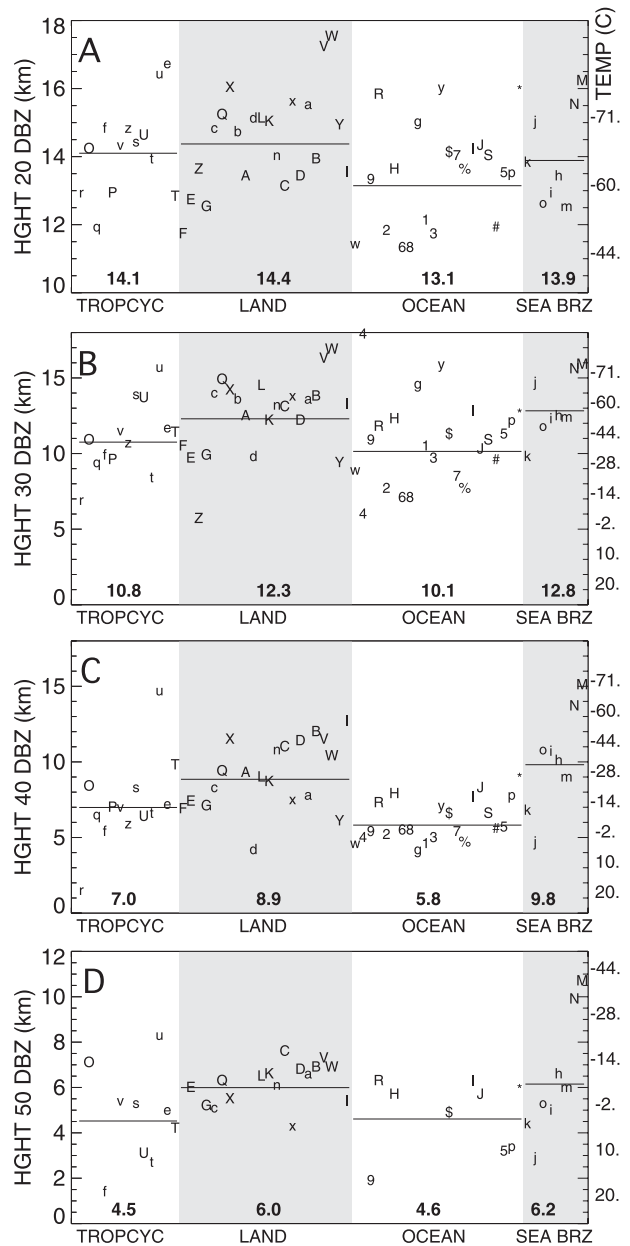


FIG. 8. As in Fig. 7, but for maximum heights for (a) 20-, (b) 30-, (c) 40-, and (d) 50-dBZ radar echoes.

1999) that were in an easterly regime mentioned earlier, have 40 dBZ up to 10 km and 30 dBZ up to 16–17-km altitude suggesting possible large graupel or hail in this storm, but no ground-based radar observations were available. We note that the EDOP measurements have high resolution compared to TRMM (<1 km versus 4 or 5 km), but they cover only one horizontal dimension and the flight line may miss the updraft or reflectivity core peak. These resolution issues have previously been discussed in Heymsfield et al. (2000), where EDOP data were degraded to the TRMM PR for assessing how well

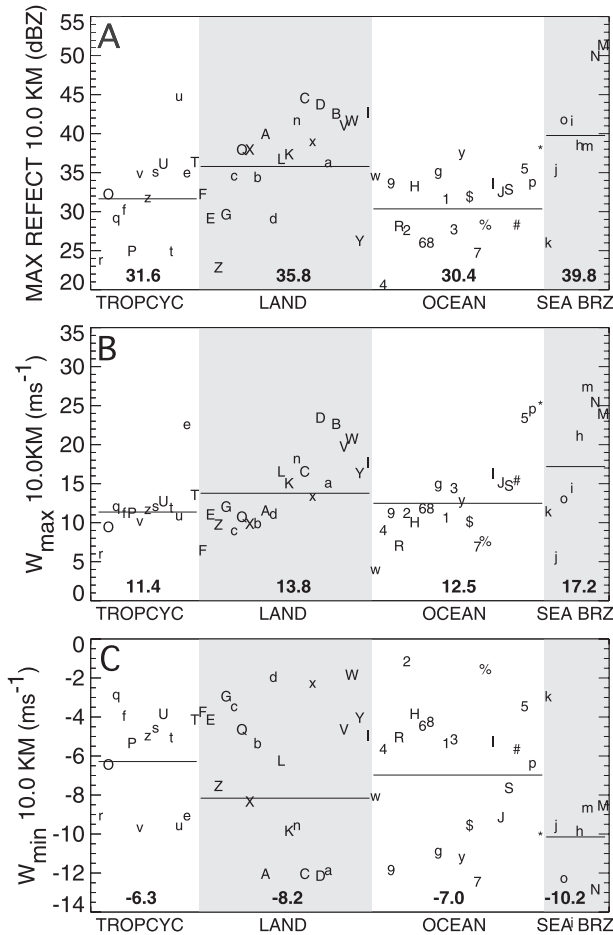


FIG. 9. As in Fig. 7, but for (a) maximum reflectivity, (b) updraft maxima, and (c) downdraft maxima, at the 10-km level for all cases.

TRMM samples convective events. TRMM generally observed weaker convective cores than EDOP because of the small size of the cores.

3) PEAK UPDRAFT/DOWNDRAFT AND REFLECTIVITY AT 10-KM ALTITUDE (FIG. 9)

This altitude is examined since it is near the $-40^{\circ}C$ level and generally below the strongest updrafts. The reflectivity (Fig. 9a) shows a significant variability among the cases with Florida sea-breeze convection. Cases M and N clearly have the highest reflectivities (~ 50 dBZ); this case was previously mentioned to have small hail detected with polarimetric radar. Hurricane Emily (case u) is the next strongest case, followed by a number of land-based storms. The means of maximum reflectivity are ~ 30 – 40 dBZ for the convection categories, with land and sea breeze having consistently higher values than the oceanic cases. The peak vertical velocities (Fig. 9b) also consistently show higher values in the land-based and sea-breeze convection. The tropical cyclone cases

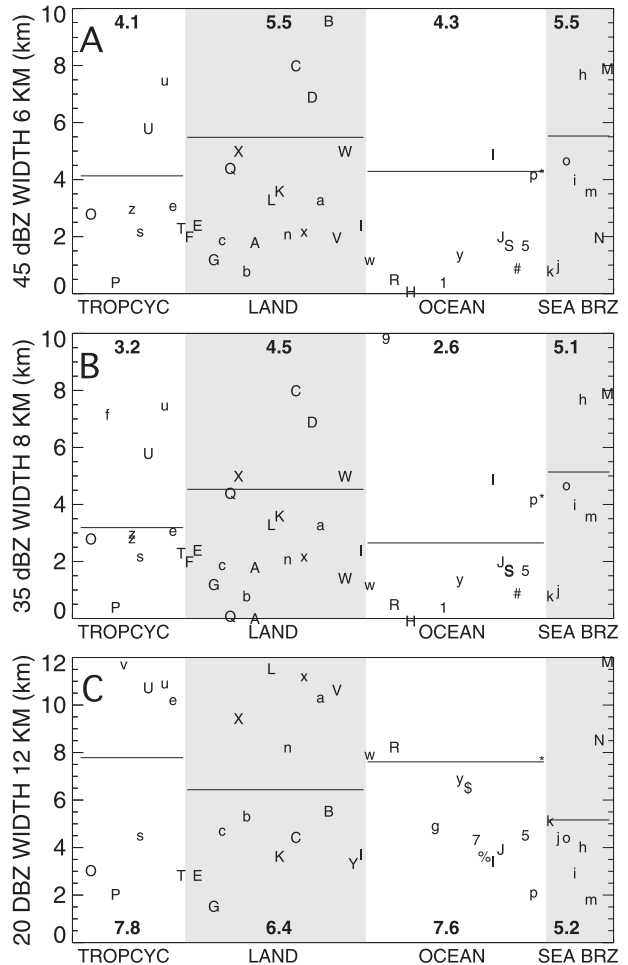


FIG. 10. As in Fig. 7, but for widths of reflectivity cores for (a) 45 dBZ at 6 km, (b) 35 dBZ at 8 km, and (c) 20 dBZ at 12 km.

consistently have ~ 12 $m s^{-1}$ updrafts with the exception of Tropical Storm Chantal (Figs. 3d and 6d; case e), which contained a 23 $m s^{-1}$ value. This value is reasonable since it is near the value observed by the NASA DC-8 aircraft during the penetration of one of the updrafts in this storm (Herman and Heymsfield 2003). Downdraft magnitudes (Fig. 9c) have peak values mostly in the 2 – 6 $m s^{-1}$ range with some values between 10 – 14 $m s^{-1}$, indicating that most of the strongest downdrafts occur above 10-km altitude (cf. Fig. 7b).

4) WIDTHS OF REFLECTIVITY CORES AT 6-, 8-, AND 12-KM ALTITUDE (FIG. 10)

It is difficult to obtain full profiles of the core reflectivity, so we have examined widths at the levels (6, 8, and 12 km) used in Figs. 2–4. The 45-dBZ widths at 6-km altitude and 35-dBZ widths at 8-km altitude range from ~ 0 to 9 km, with land-based cores significantly wider than that for the oceanic and tropical cyclone categories

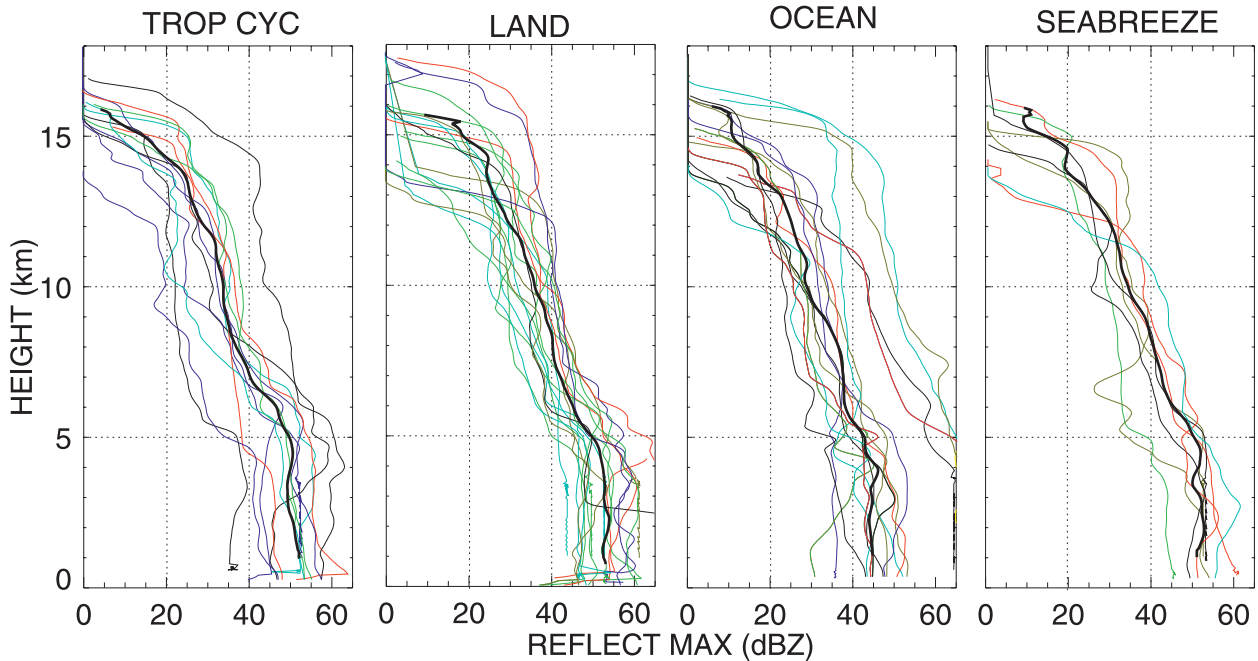


FIG. 11. Comparison of maximum reflectivity profiles sorted into four categories of convection. Individual (nonblack) profiles are from each case in Table 2; black curves are mean in each class. Dotted lines are provided for reference.

($\sim 4\text{--}5$ versus ~ 1.8 km). The width of the 20-dBZ core at 12 km, the upper-level anvil outflow, also has considerable variability in core width ($\sim 0.5\text{--}9$ km), but all widths have broadened to $\sim 5\text{--}6$ km in the mean. Anderson et al. (2005; see also references therein) found that updraft cores (based on vertical velocities) during various tropical field programs had median widths of ~ 1 km and top 10% core widths from ~ 1.5 to 4 km (~ 4 to 6 km) for nonhurricane (hurricane) cases; core widths increased slightly with height from near-surface to 9-km altitude. Their cases were biased toward weaker updrafts that could safely be penetrated by aircraft, but the observations here are reflectivity core widths, which would be expected to be larger and less well defined than vertical velocity. EDOP-derived widths in this paper may also be exaggerated since the radar beam acts much like a filter, so features less than the beamwidth may be smeared out.

b. Vertical profiles

Vertical profiles of peak reflectivity and peak updraft and downdraft magnitudes, sorted by convection category are shown in Figs. 11–13. For example, the rightmost curves in Figs. 5a,d and 6a,d were used for peak values of reflectivity and updraft for those cases, and the leftmost curves in Figs. 5d and 6d were used for peak downdrafts. Each profile is from a different case in

Table 2 and the group of profiles does not represent a “typical profile” but rather a variety of different events. Individual curves are not identified by case since it would be difficult to discern in the figure; the bold black curves are the mean curve for each class. All reflectivity profiles (Fig. 11) show a strong decrease with increasing altitude above the freezing level. Two extreme cases (cases N and u on the rightmost curves in the oceanic and tropical cyclone panels) have significantly higher reflectivities aloft.

The mean profiles (Fig. 11) show that the land profile is a few dB higher than all the other profiles, and the oceanic profile is the weakest of all other profiles. Szoke et al. (1986) compared reflectivity profiles of GATE tropical convection, New England showers, and hurricanes (see their Fig. 12) and have shown a similar decrease of reflectivity with increasing height. Hail and tornadic storms were the only profiles with 50 dBZ from the surface to the freezing level, and 50 dBZ reached 10-km altitude only for tornadic storms. Profiles in Fig. 11 in general have much higher reflectivities than in Szoke et al. (1986), possibly because of the higher resolution of the aircraft measurements as well as a higher accuracy calibration. Other differences may result from the fact that their study screened storms according to near-surface reflectivity, which probably included several storms that were weaker than those in this dataset. Also, Szoke et al. plot mean reflectivity rather than peak reflectivity, which would result in lower values. There is not as

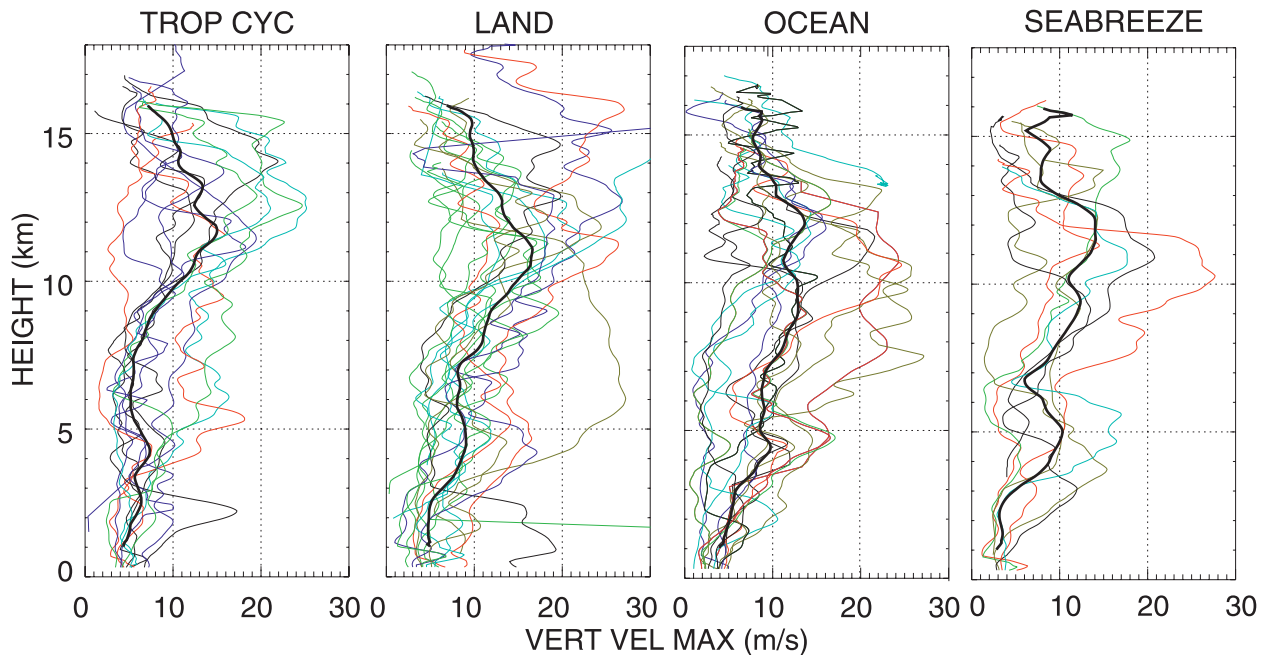


FIG. 12. As in Fig. 11, but for peak updraft magnitudes.

significant a difference in the reflectivity profiles in the present study as would be expected with convection of different types and locations.

One very interesting observation is that the reflectivities in the majority of cases decrease rapidly above 5- or 6-km altitude, where 6 km is roughly the -10°C level. Stith et al. (2002, 2004) found from in situ measurements

in the Amazon and Kwajalein that most of the updrafts glaciated rapidly, removing most of the supercooled liquid water between -5° and -17°C . This is consistent with our observations since reflectivities will be much lower in the ice phase, as mentioned earlier.

The peak vertical velocity profiles (Fig. 12) show large variability in mid to upper levels for all convection

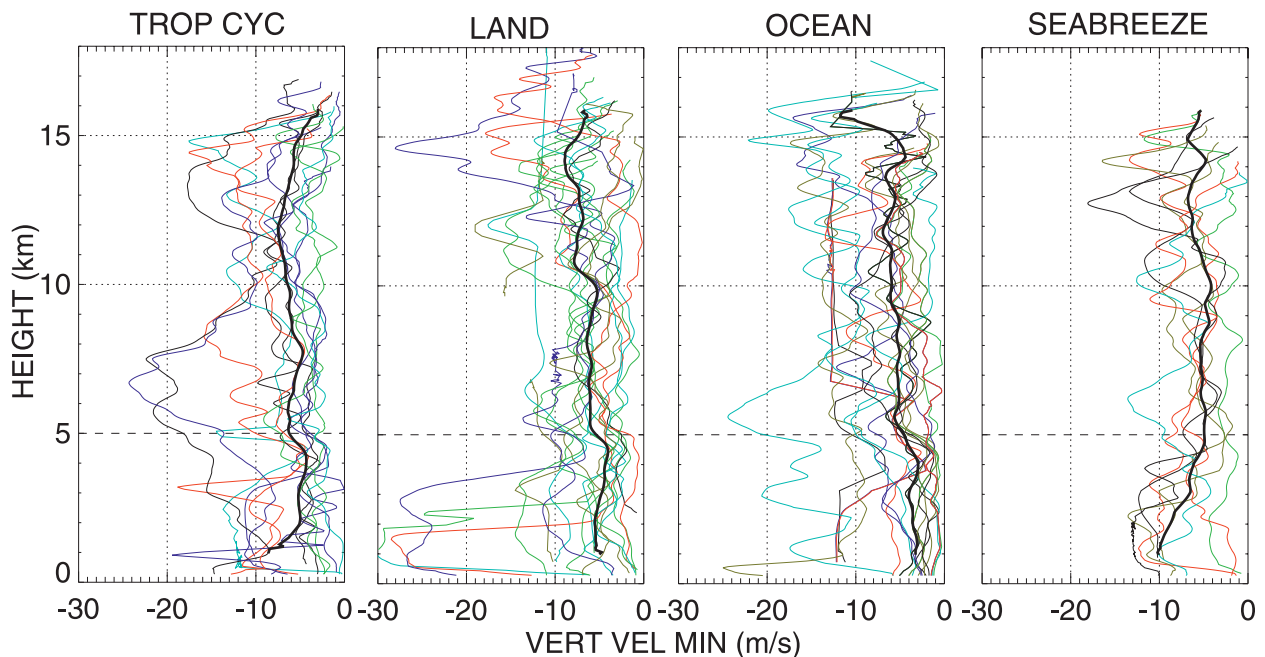


FIG. 13. As in Fig. 11, but for peak downdraft magnitudes.

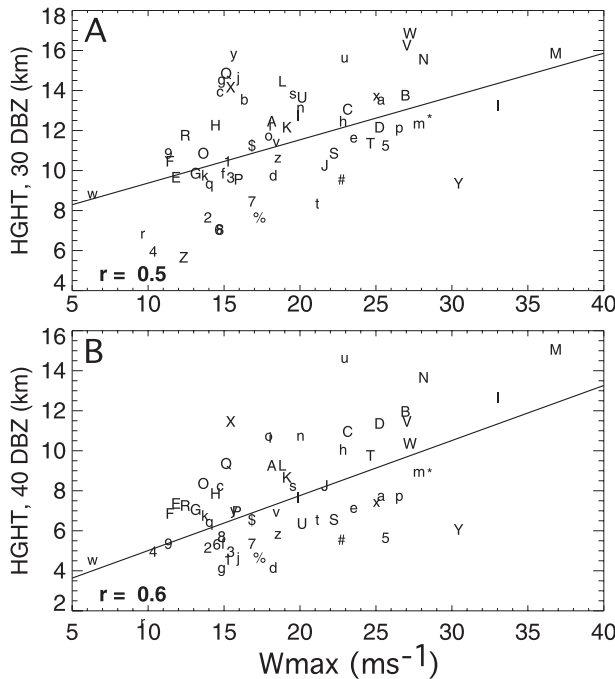


FIG. 14. Relation between w_{\max} and maximum heights attained by (a) 30- and (b) 40-dBZ reflectivity contours. Symbols for individual cases are from Table 2. Linear fit and correlation coefficient r are provided in each plot.

categories. The heights of the maximum vertical velocities in the oceanic and tropical cyclone profiles are generally higher than that of the land and sea-breeze convection cases, as noted earlier. The mean profiles depict an increase of vertical velocity from a few meters per second near the surface to $\sim 10 \text{ m s}^{-1}$ at 5-km altitude ($\sim 0^\circ\text{C}$), a minimum near 6–7-km altitude, and then another increase up to the maximum in the profile above 10-km altitude (except for the oceanic profile that has a dip to 10 m s^{-1} at 10-km altitude). The updrafts vary widely in behavior because of a combination of varied environmental conditions mentioned in the introduction and also the evolution of the cells. We will discuss their general behavior in section 4.

The downdrafts in Fig. 13 are more widely varied than the updrafts. The mean downdraft in the land and oceanic cases increase with altitude from about 5 m s^{-1} near the surface to $8\text{--}10 \text{ m s}^{-1}$ near the 15-km level; the peak downdrafts in tropical cyclones are more uniform with height with a mean value of approximately $6\text{--}7 \text{ m s}^{-1}$. There were some very strong downdrafts in the tropical cyclone cases. A few of the land convection cases had extremely large downdrafts that are suspicious since this was from one of the oldest datasets among the first EDOP measurements. These data were included in the averaging but did not appear to have

much effect on the mean curves when the entire profile was removed.

c. Satellite implications

Satellite studies of deep convection using TRMM observations have used the height of reflectivity contours as a proxy for convection intensity (e.g., Zipser et al. 2006 and references therein). Intensity of convection is largely based on updraft strength but this is not available from satellite measurements. As noted earlier, the resolution of EDOP measurements is a factor of 5 to 10 higher than the satellite TRMM PR measurements. The approach here is to look for physical relationships in the higher-resolution EDOP measurements and then use them to validate previous published inferences from TRMM PR reflectivity-only measurements that may have under sampled convection. Figure 14 provides plots for the 30- and 40-dBZ echo height (Figs. 14a,b) versus maximum updraft strength. Our sample is biased toward strong to intense convection; the plots show some correlation 0.5 (0.6) for 30 (40) dBZ, but with considerable scatter due to the varied environmental conditions and the life cycle stage of the convection, as mentioned earlier. Nevertheless, when 30-dBZ echoes are at or above 10-km altitude, it is likely that the updrafts are at least $10\text{--}12 \text{ m s}^{-1}$, if not significantly stronger. When the 40-dBZ echo is above 10 km, most of the updrafts are $>15 \text{ m s}^{-1}$. This is useful information for the TRMM Precipitation Radar since it attaches some significance of using reflectivity heights as a proxy for updraft strength. It is also useful information since estimation of latent heat with updrafts based on reflectivity may have a large error because our observations indicate that strong updrafts are not always correlated with high reflectivity.

4. Discussion of convection statistics

Figure 15 compares the mean profiles of peak values for the different categories of convection. The most notable differences in the figure are the following: 1) the oceanic reflectivity profile is at least 5 dBZ lower than that of the other reflectivity profiles; 2) the tropical cyclone convection vertical velocities are lowest at mid-levels but still have comparable maxima to all other cases except the land-based convection; and 3) the updrafts increase to about 10 m s^{-1} near the melting level and they are very similar between cases. These observations pose several very interesting questions related to the dynamics and microphysics of tropical convection: Why do the updraft peaks often have a bimodal structure with a low-level ($<6 \text{ km}$) and an upper-level ($>10 \text{ km}$) peak? Why are the updraft maxima often above 10-km altitude?

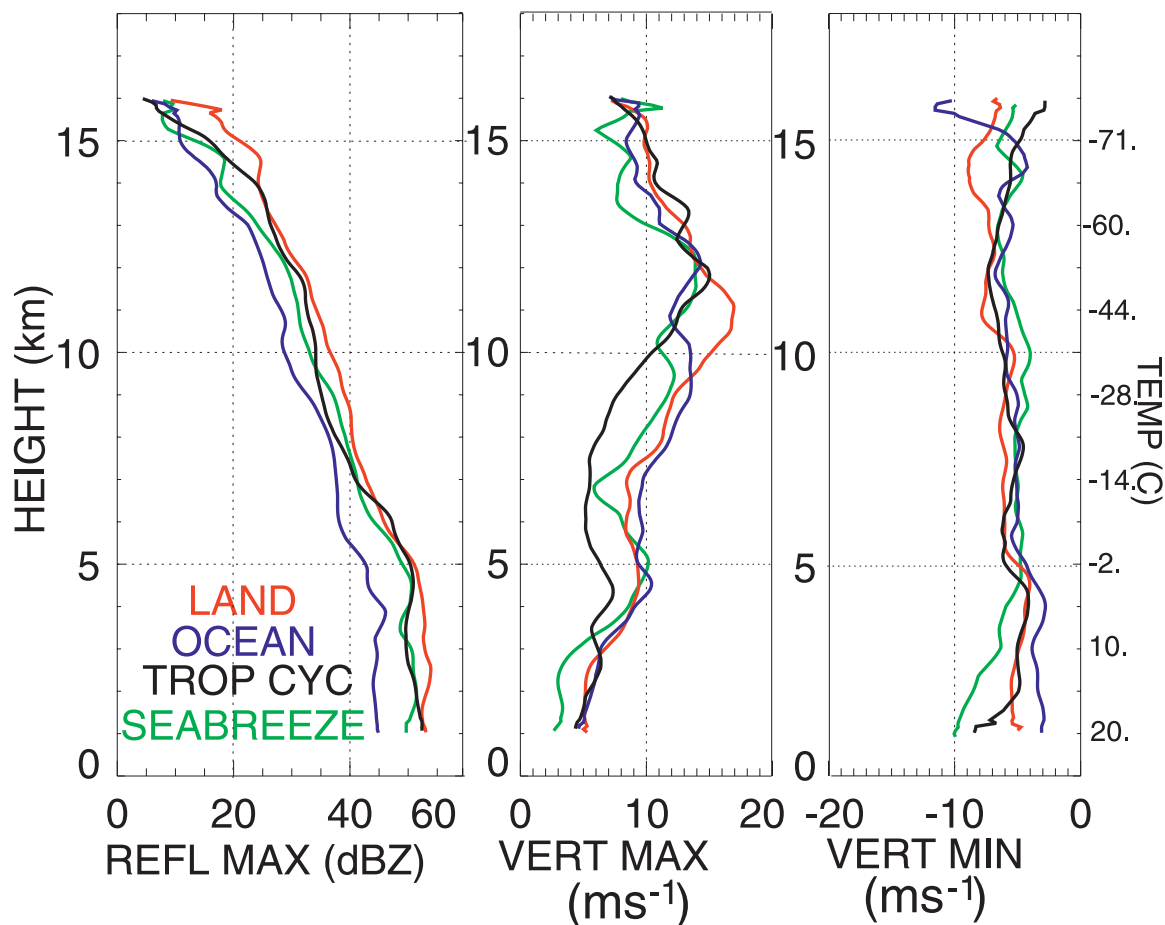


FIG. 15. Mean profiles for land, ocean, tropical cyclone, and sea-breeze convection types that summarize Figs. 11–13. Temperature scale from Jordan mean sounding is shown on right side of figure.

Work by Zipser (2003) and Fierro et al. (2009) suggests that both the effects of release of latent heat of freezing and precipitation unloading well above the freezing level provides a boost to the updraft that may be responsible for higher updraft speeds aloft. Fierro et al. (2009) studied this process using a cloud model and suggested that the original hot tower hypothesis that postulated undiluted towers should be modified to include mixing. They further suggest that the boost from latent heat of freezing compensates the effects of mixing at lower levels.

The microphysics is critical toward understanding the above questions. Heymsfield et al. (2009) used an assemblage of in situ penetrations of maritime updrafts and showed that most of the condensate is removed before reaching the -20°C level in low-latitude updrafts and the amount continues to diminish upward in the updrafts. Even with vigorous updrafts, large ice can fall out of tilted updrafts or from mixing near the updraft edge, which can reduce vertical velocities. The decrease of the reflectivity with height implies a decrease in ice

water content similar to that observed in Heymsfield et al. (2009), suggesting significant loss of hydrometeor mass with altitude. The reflectivity profiles in Fig. 11 further support this view.

With this in mind, the general behavior of the observed updraft profiles can be described as follows. As raindrops grow above cloud base while ascending to the 0°C level (or -10°C level if supercooled), latent heating from condensation provides buoyancy for the updraft. Drag from rain progressively loads down the updrafts with height just above the 0°C level, as suggested by the slight minima observed in the observations (Fig. 15) just above the 0°C level (5 to 6 km). Updrafts strengthen above 6–7 km after they fall out of hydrometeors, which reduces the precipitation load in the updraft. Any remaining supercooled cloud drops will freeze by the homogeneous nucleation (temperatures $< -38^{\circ}\text{C}$, ~ 10 km) (Heymsfield et al. 2009), resulting in additional updraft buoyancy through latent heating of freezing (Fierro et al. 2009). The complexity of these processes requires further study

since there are several competing processes that require better observations and improvements in microphysics parameterizations in numerical models.

5. Summary and conclusions

This paper has presented vertical motion and reflectivity structure from a multiyear set of observations of convection from NASA field experiments in diverse environments in the tropics and subtropics. The measurements were obtained from the nadir-viewing EDOP radar on the high-altitude NASA ER-2 aircraft. This study is the first time that updrafts, particularly oceanic, have been examined in such detail through their full vertical extent. Four types of convection were defined in the paper (tropical cyclone, land-based, oceanic, and sea breeze) based on the cases studied. A number of interesting features were obtained from the analyses of reflectivity and vertical motions, providing insights into the kinematic and microphysical processes that are otherwise difficult to obtain.

It was found that both updrafts and downdrafts in deep land-based and oceanic convective storms are quite strong, with peak updraft values often exceeding 15 m s^{-1} and the height of the peak often above 10-km altitude; sometimes a second smaller peak in the vertical velocity was present near the freezing level. The land-based and sea-breeze storms had slightly stronger updrafts than the oceanic and tropical cyclone convection cases. The heights of peak updrafts for tropical cyclones were 1–2 km higher than that of the other convection types. These results confirm earlier case studies of tropical convection with double-peaked updrafts with the smaller peak at lower levels and the larger peak at higher altitudes (e.g., Jorgensen et al. 1997), but the updraft magnitudes in the current study are generally much larger because of the higher resolution of the measurements. The strong downdrafts at upper levels are associated with strong updrafts, and their intensity also appears to be correlated. The downdraft dynamics are complex and require further study. The reflectivity profiles showed that oceanic convection had lower reflectivities in general compared to other categories of convection, confirming earlier results from Szoke et al. (1986) and others; one tropical cyclone and one sea-breeze case clearly stood out from the other cases as being extreme. The tropical cyclone convection had peak updrafts at about the 12-km level, a few kilometers higher than that for the other convection types. However, the tropical cyclone cases had the weakest midlevel updrafts. The convection studied in this paper is biased toward certain tropical and subtropical meteorological situations. In the future, we hope to obtain

similar types of datasets for higher-latitude continental convection to help in understanding dynamical and microphysical similarities, if they exist, with the current study.

Vertical velocity is a key unknown measurement from the TRMM and future GPM satellites whose mission is not only to measure tropical rainfall but also to estimate heat budgets in precipitation. In this study, we used the reflectivity and vertical motions to explore the relationship between high reflectivities aloft and the strength of updrafts. A correlation of 0.6 (0.5) was found between the height of the 40 dBZ (30 dBZ) reflectivity and vertical velocity. It is likely that this lack of correlation in some cases is due to the evolution of the convection (i.e., the phasing of the reflectivity and vertical motion), where strongest updrafts often occur during early development of cells and the highest reflectivities and strongest downdrafts occur during the mature to dissipation of the cell. This has implications for satellite retrievals that capture an instant during the lifetime of a convective event. It would appear that intensity estimates from convection with weaker reflectivities over land by TRMM would be more difficult; furthermore, latent heating estimates based on these have much larger uncertainties.

This study has focused mainly on characterizing the radar measurements and not on the convective environment (i.e., CAPE, vertical shear, or other pertinent parameters). We have not presented a discussion of entrainment in this paper even though the peak updraft profiles suggest strong convergence and possibly entrainment in midlevels. These subjects will be explored in future efforts through a more rigorous examination of the dynamics and microphysics that produce the general behavior of the observed updraft and reflectivity profiles. Finally, the vertical velocity magnitudes at higher altitudes near the storm top are quite strong, suggesting safety concerns for high-altitude UAS such as the Global Hawk that will fly near the 18-km altitude level for hurricane reconnaissance. Convection frequently overshoots the tropopause in a number of the cases studied, with altitudes reaching 15–18 km.

Acknowledgments. This work was supported by Dr. Ramesh Kakar of NASA's Atmospheric Dynamics Program. Some of the data collection and analysis were sponsored by the NASA Radiation Sciences Program (CRYSTAL-FACE and TC4). We are greatly appreciative of Jeff Caylor, Steve Bidwell, Ed Zenker, and Larry Belcher, and others for the many years of hard work on the radar hardware and data processing required for obtaining the high-quality data sets in this study. We are greatly appreciative of Professor Ed Zipser of the University of

Utah for his significant effort leading many of the field experiments used in this paper and for his comments on the paper. We are also appreciative of two anonymous reviewers who provided constructive comments on the manuscript, and to Dr. Dan Cecil of University of Alabama in Huntsville for corrections on the manuscript.

APPENDIX

Fall Speed Calculations

Calculation of vertical velocity w from EDOP nadir Doppler velocity v_d observations requires estimation of the reflectivity weighted fall velocity v_f at each grid point as in Heymsfield et al. (1999; hereafter H99). The v_f estimation is the most critical assumption in obtaining w since v_f depends on many factors such as particle phase, particle size distribution, ice particle habit, etc. In H99, stratiform regions are separated vertically into three regions: rain, snow, and a transitional region corresponding to the melting layer. The approach is modified from previous papers (Marks and Houze 1987; Black et al. 1996) that use reflectivity– v_f relations for snow, rain, transition (melting), and convective regions. The H99 approach was modified for EDOP observations using a more realistic rain reflectivity– v_f relation derived for a gamma distribution (Ulbrich and Chilson 1994) and using a parabolic profile in the transition region instead of a linear one. Based on these more recent microphysical observations, the H99 fall speed estimates are modified with 1) an improved fall speed relation for the ice phase and 2) more realistic representation of the raindrop freezing level in strong convection.

Difficulties with fall speed estimation occur in mixed phase regions associated with convection where strong updrafts can loft liquid water, frozen raindrops, and graupel several kilometers above the melting level. In situ aircraft are often unable for safety reasons to fly through strong convection where graupel and hail may be present. Black et al. (1986) documented hurricane microphysics with the WP-3D aircraft and found that convection was almost completely glaciated above the -5°C level and that millimeter-diameter graupel was common. Black et al. (2003) observed from probe data 2–3-mm spherical particles at 12-km altitude (-40°C) of a hot tower in Hurricane Bonnie. These particles were suggested to be a mixture of ice and supercooled raindrops. Raindrops for this size and altitude would have fall speeds of $\sim 13\text{ m s}^{-1}$ at 12-km altitude. Herman and Heymsfield (2003) found millimeter-size slushy particles in Tropical Storm Chantal, also near the -40°C level. Previous tropical and hurricane observations did not

indicate high-density ice (i.e., hail), so it is not considered in the current study since it is unlikely that it is present in the majority of the cases presented.

The snow fall speeds previously used are underestimates for graupel, which can have significantly higher fall speeds, resulting in w errors of several meters per second or more in convective regions. An additional factor is that raindrops in convection may become supercooled in updrafts and freeze at -10° to -20°C (7–8-km altitudes). Stith et al. (2002, 2004) found that most supercooled water in convection was found at temperatures warmer than -12°C in strong updrafts, although some was found at temperatures as cold as -18°C . They examined frozen and unfrozen raindrops, the majority of which were less than 1 mm. Small coexisting cloud droplets can freeze at much lower temperatures (e.g., -35°C) by homogeneous nucleation (Heymsfield et al. 2005). We use this knowledge to obtain a more realistic fall speed relation, knowing that one relation will never satisfy all the possible microphysical scenarios.

The fall speeds for the ice phase, v_{if} are derived from a combination of snow in situ measurements derived from the Cirrus Regional Study of Tropical Anvils and Cirrus Layers–Florida–Area Cirrus Experiment (CRYSTAL-FACE, hereafter C-F) convection measurements in Florida (Heymsfield et al. 2004) and theoretical calculations for graupel based on limited observations. For the snow calculations, in situ particle size distributions were used from all cases during C-F that consisted of an assortment of stratiform and convection cases mainly over maritime areas with some over land. From the C-F size distributions and size-dependent ice densities that were constrained by direct measurements of the IWC, radar reflectivity was calculated at 9.6 GHz (EDOP frequency) using the Bohren and Huffman (1983) Mie scattering equations for spherical ice hydrometeors. Taking the same densities and projected particle areas from 2D probe images, snow fall speeds v_s were calculated (Mitchell and Heymsfield 2005). Mean reflectivity-weighted fall speeds (V_Z) were then calculated using the above scattering algorithm. Relationships between Z_e and V_Z were derived. The resulting calculated 9.6-GHz Doppler velocities versus reflectivity are shown in Fig. A1a for all C-F cases for the 1000-hPa (surface) pressure level. The reflectivities range from less than -10 to 29 dBZ and a linear curve ($-3.4 + 0.19\text{ dBZ}$) is fitted to the snow points as shown in the figure.

The graupel fall speeds v_G were calculated based on theory and limited observations. Size distributions are taken to be exponentials, $N = N_0 e^{-\lambda D}$, where N_0 is taken as 0.1 or 0.01 cm^{-3} to bound values used in earlier studies (Braun and Tao 2000), D is particle diameter, and λ is the slope of the size distribution; N_0 is taken to be

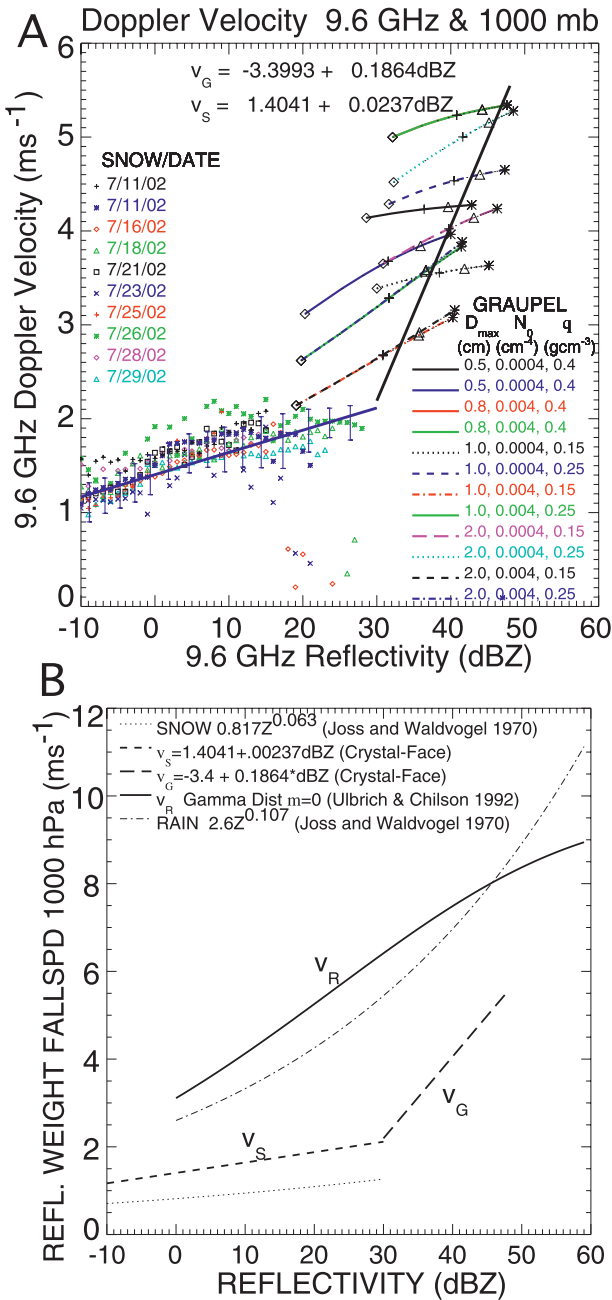


FIG. A1. Fall speed relations. (a) Snow fall speeds based on in situ observations and theoretical graupel fall speeds based on observed graupel characteristics. The symbols for snow (<30 dBZ) each represent an average of all points for a single flight in 1-dBZ intervals. IWC increases from 0.01 to 2 g m^{-3} on the graupel curves on the right side of the plot. Linear fits (black solid curves) are given for the snow and graupel points; the graupel fit is through $\text{IWC} = 1 \text{ g m}^{-3}$ points. (b) Fall speed relations used in Doppler velocity-derived vertical velocities.

0.01 cm^{-4} as a lower bound. Ice density (ρ) at temperatures below -10°C have been assumed to be 0.15 g cm^{-3} , which was found as the ensemble mean for heavily rimed particles for a typical C-F updraft (Heymsfield et al. 2005); 0.4 g cm^{-3} from wind tunnel observations of Pflaum and Pruppacher (1979) and Knight and Heymsfield (1983); and 0.25 g cm^{-3} as an intermediate value. For an exponential distribution, $\text{IWC} = N_0 \rho \Gamma(4)/\lambda^4$. Ice water content (IWC) is specified from 0.01 to 2 g cm^{-3} based on C-F observations, and N_0 is adjusted to give the correct IWC with the maximum diameters D_{max} assumption chosen as 0.5, 0, 8, 1.2, and 2 cm from C-F and other observations. Radar reflectivity for graupel is calculated similar to snow. Figure A1a shows the relations calculated for the various D_{max} , N_0 , and ρ above. A linear curve is fitted through $\text{IWC} = 1 \text{ g m}^{-3}$ points on each of the graupel curves.

The above relations for v_S and v_G apply to ground level (1000 hPa). Fall speeds at other altitudes are obtained by multiplying by $[\rho_o/\rho]^x$, where ρ and ρ_o are the air density at the surface and measurement height, respectively, and x varies from 0.4 to 0.45 depending on rain rate and other factors (Beard 1976, 1985); here we assume 0.45. The above fall speed relations are at the surface and must be multiplied by this correction factor. The Jordan mean tropical sounding was used for all cases except the HOPEX Louisiana convection winter cases; nearby soundings were used for these midlatitude cases where the freezing level was at approximately 3.2 km.

Figure A1b shows the three fall speed curves (v_R , v_S , and v_G) used in the paper. Also shown are a few other well-referenced fall speed curves for comparison. A diagram describing the calculation of reflectivity-weighted fall speed estimates is given in Fig. A2. The main changes here from H99 are the v_i calculation and the transitioning between rain and snow or graupel between 6 and 8 km in convective cores. Using the curves in Fig. A1b for the EDOP fall speed correction would likely have an uncertainty less than $1\text{--}2 \text{ m s}^{-1}$ for most cases based on the above discussion. Uncertainties in fall speed estimates may arise because of the presence of higher-density hail or frozen raindrops that we are not accounting for or from improper attenuation corrections of the data. Hail would result in an underestimated fall speed by 5 m s^{-1} or more and would cause vertical velocities to be underestimated. Attenuation corrections mainly occur for reflectivities $>40 \text{ dBZ}$ and they are most significant at lower levels ($<6 \text{ km}$) in the rain regions of convective cores. At these levels, an error in reflectivity would result in a few meters per second error in rain fall speed and vertical velocity. Another source of error would be cases where there is supercooled water and frozen

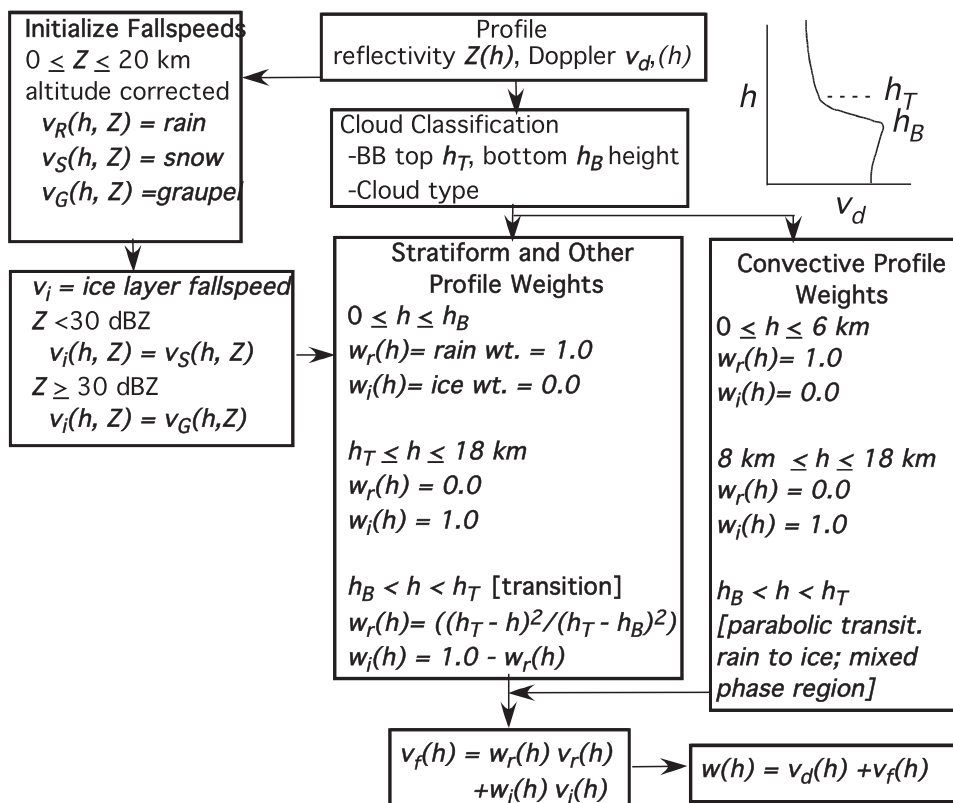
REFLECTIVITY-WEIGHTED FALLSPEED v_f & VERTICAL VELOCITY w 

FIG. A2. Fall speed and vertical velocity calculation.

raindrops in the convective cores, as observed in Stith et al. (2004). The transition between rain and ice has been increased in altitude so that it is between the 6- and 8-km level to account for supercooled water. We have not accounted for frozen raindrops, which will have higher fall velocities than graupel.

We attempted to examine the uncertainty in the EDOP-derived vertical velocity for cases in which we underestimate fall speeds, such as if frozen drops rather than graupel were present. We assumed rain fall speeds (Fig. A2, v_R) instead of graupel fall speeds since these will provide a rough upper bound for what we would expect for 1-mm frozen drops. The resulting plots were compared to those calculated with using graupel fall speeds. The resulting fall speeds and peak vertical velocities were typically 2–5 m s^{-1} higher than for graupel, the height of the updraft maxima were within a few tenths of a kilometer of those with the graupel calculation, and the downdrafts were affected less than 1 m s^{-1} . We therefore conclude that the larger fall speeds associated with frozen raindrops will have a minor effect on the overall vertical velocity results in the paper. We are likely biased low on updraft speeds if hail or frozen drops are present.

REFERENCES

- Adler, R. F., and R. A. Mack, 1986: Thunderstorm cloud-top dynamics as inferred from satellite observations and a cloud-top parcel model. *J. Atmos. Sci.*, **43**, 1945–1960.
- Anderson, N. F., C. A. Grainger, and J. L. Stith, 2005: Characteristics of strong updrafts in precipitation systems over the central tropical Pacific Ocean and in the Amazon. *J. Appl. Meteor.*, **44**, 731–738.
- Battan, L. J., 1973: *Radar Observation of the Atmosphere*. University of Chicago Press, 324 pp.
- Beard, K. V., 1976: Terminal velocity and shape of cloud and precipitation drops aloft. *J. Atmos. Sci.*, **33**, 851–864.
- , 1985: Simple altitude adjustments to raindrop velocities for Doppler analysis. *J. Atmos. Oceanic Technol.*, **2**, 468–471.
- Black, M. L., R. W. Burpee, and F. D. Marks Jr., 1996: Vertical motion characteristics of tropical cyclones determined with airborne Doppler radial velocities. *J. Atmos. Sci.*, **53**, 1887–1909.
- Black, P. G., R. A. Black, J. Hallett, and W. A. Lyons, 1986: Electrical activity on the hurricane. Preprints, *23rd Conf. on Radar Meteorology*, Snomass, CO, Amer. Meteor. Soc., J277–J280.
- Black, R. A., G. M. Heymsfield, and J. Hallett, 2003: Extra large particle images at 12 km in a hurricane eyewall: Evidence of high-altitude supercooled water? *Geophys. Res. Lett.*, **30**, 2124, doi:10.1029/2003GL017864.
- Bohren, C. F., and D. R. Huffman, 1983: *Absorption and Scattering of Light by Small Particles*. Wiley, 530 pp.

- Braun, S. A., and W.-K. Tao, 2000: Sensitivity of high-resolution simulations of Hurricane Bob (1991) to planetary boundary layer parameterizations. *Mon. Wea. Rev.*, **128**, 3941–3961.
- Cecil, D. J., S. J. Goodman, D. J. Bocippio, E. J. Zipser, and S. W. Nesbitt, 2005: Three years of TRMM precipitation features. Part I: Radar, radiometric, and lightning characteristics. *Mon. Wea. Rev.*, **133**, 543–566.
- Fierro, A. O., J. M. Simpson, M. A. LeMone, J. M. Straka, and B. F. Smull, 2009: On how hot towers fuel the Hadley cell: An observational and modeling study of line-organized convection in the equatorial trough from TOGA COARE. *J. Atmos. Sci.*, **66**, 2730–2746.
- Geerts, B., G. M. Heymsfield, L. Tian, J. B. Halverson, A. Guillory, and M. I. Mejia, 2000: Hurricane Georges's landfall in the Dominican Republic: Detailed airborne Doppler radar imagery. *Bull. Amer. Meteor. Soc.*, **81**, 999–1018.
- Guimond, S. R., G. M. Heymsfield, and F. J. Turk, 2010: Multi-scale observations of Hurricane Dennis (2005): The effects of hot towers on rapid intensification. *J. Atmos. Sci.*, in press.
- Halverson, J., and Coauthors, 2007: NASA's Tropical Cloud Systems and Processes Experiment: Investigating tropical cyclogenesis and hurricane intensity change. *Bull. Amer. Meteor. Soc.*, **88**, 867–882.
- Herman, R. L., and A. J. Heymsfield, 2003: Aircraft icing at low temperatures in Tropical Storm Chantal (2001). *Geophys. Res. Lett.*, **30**, 1955, doi:10.1029/2003GL017746.
- Heymsfield, A. J., A. Bansemer, C. Schmitt, C. Twohy, and M. R. Poellot, 2004: Effective ice particle densities derived from aircraft data. *J. Atmos. Sci.*, **61**, 982–1003.
- , L. M. Miloshevich, C. Schmitt, A. Bansemer, C. Twohy, M. R. Poellot, A. Fridland, and H. Gerber, 2005: Homogeneous ice nucleation in subtropical and tropical convection and its influence on cirrus anvil microphysics. *J. Atmos. Sci.*, **62**, 41–64.
- , A. Bansemer, G. Heymsfield, and A. Fierro, 2009: Microphysics of maritime tropical convective updrafts at temperatures from -20° to -60°C . *J. Atmos. Sci.*, **66**, 3530–3562.
- Heymsfield, G. M., 1989: Accuracy of vertical air motions from nadir-viewing Doppler airborne radars. *J. Atmos. Oceanic Technol.*, **6**, 1079–1082.
- , and S. Schotz, 1985: Structure and evolution of a severe squall line over Oklahoma. *Mon. Wea. Rev.*, **113**, 1563–1589.
- , R. Fulton, and J. Spinhirne, 1991: Aircraft overflight measurements of Midwest severe thunderstorms: Implications of geosynchronous satellite interpretations. *Mon. Wea. Rev.*, **119**, 436–456.
- , and Coauthors, 1996: The EDOP radar system on the high-altitude NASA ER-2 aircraft. *J. Atmos. Oceanic Technol.*, **13**, 795–809.
- , J. B. Halverson, and I. J. Caylor, 1999: A wintertime Gulf coast squall line observed by EDOP airborne Doppler radar. *Mon. Wea. Rev.*, **127**, 2928–2950.
- , B. Geerts, and L. Tian, 2000: TRMM precipitation radar reflectivity profiles as compared with high-resolution airborne and ground-based measurements. *J. Appl. Meteor.*, **39**, 2080–2102.
- , J. B. Halverson, J. Simpson, L. Tian, and P. Bui, 2001: ER-2 Doppler radar (EDOP) investigations of the eyewall of Hurricane Bonnie during the Convection and Moisture Experiment-3. *J. Appl. Meteor.*, **40**, 1310–1330.
- , —, E. Ritchie, J. Simpson, J. Molinari, and L. Tian, 2006: Structure of highly sheared Tropical Storm Chantal during CAMEX-4. *J. Atmos. Sci.*, **63**, 268–287.
- Houze, R. A., Jr., W.-C. Lee, and M. M. Bell, 2009: Convective contribution to the genesis of Hurricane Ophelia (2005). *Mon. Wea. Rev.*, **137**, 2778–2800.
- Iguchi, T., and R. Meneghini, 1994: Intercomparison of single-frequency methods for retrieving a vertical rain profile from airborne or spaceborne radar data. *J. Atmos. Oceanic Technol.*, **11**, 1507–1516.
- Jenkins, G. S., A. Pratt, and A. Heymsfield, 2008: Possible linkages between Saharan dust and tropical cyclone rain band invigoration in the eastern Atlantic during NAMMA-06. *Geophys. Res. Lett.*, **35**, L08815, doi:10.1029/2008GL034072.
- Jensen, E., D. Starr, and O. Toon, 2004: Mission investigates tropical cirrus clouds. *Eos, Trans. Amer. Geophys. Union*, **85**, 45–50.
- Johnson, R. H., S. L. Aves, P. E. Ciesielski, and T. D. Keenan, 2005: Organization of oceanic convection during the onset of the 1998 East Asian summer monsoon. *Mon. Wea. Rev.*, **133**, 131–148.
- Jorgensen, D. P., and M. A. LeMone, 1989: Vertical velocity characteristics of oceanic convection. *J. Atmos. Sci.*, **46**, 621–640.
- , E. J. Zipser, and M. A. LeMone, 1985: Vertical motions in intense hurricanes. *J. Atmos. Sci.*, **42**, 839–856.
- , M. A. LeMone, and S. B. Trier, 1997: Structure and evolution of the 22 February 1993 TOGA COARE squall line: Aircraft observations of structure, circulation, and surface energy fluxes. *J. Atmos. Sci.*, **54**, 1961–1985.
- Kakar, R., M. Goodman, R. Hood, and A. Guillory, 2006: Overview of the Convection and Moisture Experiment (CAMEX). *J. Atmos. Sci.*, **63**, 5–18.
- Knight, N. C., and A. J. Heymsfield, 1983: Measurement and interpretation of hailstone density and terminal velocity. *J. Atmos. Sci.*, **40**, 1510–1516.
- Lang, S., W.-K. Tao, R. Cifelli, W. Olson, J. Halverson, S. Rutledge, and J. Simpson, 2007: Improving simulations of convective systems from TRMM LBA: Easterly and westerly regimes. *J. Atmos. Sci.*, **64**, 1141–1164.
- LeMone, M. A., and E. J. Zipser, 1980: Cumulonimbus vertical velocity events in GATE. Part I: Diameter, intensity and mass flux. *J. Atmos. Sci.*, **37**, 2444–2457.
- , T. Y. Chang, and C. Lucas, 1994: On the effects of filtering on convective-core statistics. *J. Atmos. Sci.*, **51**, 3344–3350.
- Lin, Y.-L., R. D. Farley, and H. D. Orville, 1983: Bulk parameterization of the snow field in a cloud model. *J. Climate Appl. Meteor.*, **22**, 1065–1092.
- Liu, C., and E. J. Zipser, 2005: Global distribution of convection penetrating the tropical tropopause. *J. Geophys. Res.*, **110**, D23104, doi:10.1029/2005JD006063.
- Lucas, C., M. A. LeMone, and E. J. Zipser, 1994a: Convective available potential energy in the environment of oceanic and continental clouds: Correction and comments. *J. Atmos. Sci.*, **51**, 3829–3830.
- , —, and —, 1994b: Vertical velocity in oceanic convection off tropical Australia. *J. Atmos. Sci.*, **51**, 3183–3193.
- Marks, F. D., and R. A. Houze Jr., 1987: Inner core structure of Hurricane Alicia from airborne Doppler radar observations. *J. Atmos. Sci.*, **44**, 1296–1317.
- May, P. T., and D. K. Rajopadhyaya, 1999: Vertical velocity characteristics of deep convection over Darwin, Australia. *Mon. Wea. Rev.*, **127**, 1056–1071.
- Mitchell, D. L., and A. J. Heymsfield, 2005: Refinements in the treatment of ice particle terminal velocities, highlighting aggregates. *J. Atmos. Sci.*, **62**, 1637–1644.

- Montgomery, M. T., M. E. Nicholls, T. A. Cram, and A. B. Saunders, 2006: A vortical hot tower route to tropical cyclogenesis. *J. Atmos. Sci.*, **63**, 355–386.
- Nesbitt, S. W., E. J. Zipser, and D. J. Cecil, 2000: A census of precipitation features in the tropics using TRMM: Radar, ice scattering, and lightning observations. *J. Climate*, **13**, 4087–4106.
- Petersen, W. A., and S. A. Rutledge, 2001: Regional variability in tropical convection: Observations from TRMM. *J. Climate*, **14**, 3566–3586.
- Pflaum, J. C., and H. R. Pruppacher, 1979: A wind tunnel investigation of the growth of graupel initiated from frozen drops. *J. Atmos. Sci.*, **36**, 680–689.
- Sherwood, S. C., and A. E. Dessler, 2000: On the control of stratospheric humidity. *Geophys. Res. Lett.*, **27**, 2513–2516.
- Simpson, J., and V. Wiggert, 1969: Models of precipitating cumulus towers. *Mon. Wea. Rev.*, **97**, 471–489.
- , C. Kummerow, W.-K. Tao, and R. F. Adler, 1996: On the Tropical Rainfall Measuring Mission (TRMM). *Meteor. Atmos. Phys.*, **60**, 19–36.
- , J. B. Halverson, B. S. Ferrier, W. A. Petersen, R. H. Simpson, R. Blakeslee, and S. L. Durden, 1998: On the role of “hot towers” in tropical cyclone formation. *Meteor. Atmos. Phys.*, **67**, 15–35.
- Smith, P., 1984: Equivalent radar reflectivity factor for snow and ice particles. *J. Climate Appl. Meteor.*, **23**, 1258–1260.
- Starr, D. O’C., 2008: Probing the mysteries of the tropopause transition layer: The TC4 experiment. *Earth Observer*, No. 20 (3), EOS Project Science Office, Greenbelt, MD, 22–27. [Available online at http://eospsos.gsfc.nasa.gov/eos_observ/pdf/May_Jun_08.pdf.]
- Stith, J. L., J. E. Dye, A. Bansemer, A. J. Heymsfield, C. A. Grainger, W. A. Petersen, and R. Cifelli, 2002: Microphysical observations of tropical clouds. *J. Appl. Meteor.*, **41**, 97–117.
- , J. A. Haggerty, A. Heymsfield, and C. A. Grainger, 2004: Microphysical characteristics of tropical updrafts in clean conditions. *J. Appl. Meteor.*, **43**, 779–794.
- Stommel, H., 1947: Entrainment of air into a cumulus cloud. *J. Meteor.*, **4**, 91–94.
- Sun, J., S. Braun, M. I. Biggerstaff, R. G. Fovell, and R. A. Houze Jr., 1994: Warm upper-level downdrafts associated with a squall line. *Mon. Wea. Rev.*, **121**, 2919–2927.
- Szoke, E. J., E. J. Zipser, and D. P. Jorgensen, 1986: A radar study of convective cells in mesoscale systems in GATE. Part I: Vertical profile statistics and comparison with hurricanes. *J. Atmos. Sci.*, **43**, 182–198.
- Tian, L., G. M. Heymsfield, and R. C. Srivastava, 2002: Measurements of attenuation with airborne and ground-based radar in convective storm over land and its microphysical implications. *J. Appl. Meteor.*, **41**, 716–733.
- Ulbrich, C. W., and P. B. Chilson, 1994: Effects of variations in precipitation size distribution and fall speed law parameters on relations between mean Doppler fall speed and reflectivity factor. *J. Atmos. Oceanic Technol.*, **11**, 1656–1663.
- Zipser, E. J., 2003: Some view on “hot towers” after 50 years of tropical field programs and two years of TRMM data. *Cloud Systems, Hurricanes, and the TRMM. Meteor. Monogr.*, No. 51, Amer. Meteor. Soc., 49–58.
- , D. J. Cecil, C. Liu, S. W. Nesbitt, and D. P. Yorty, 2006: Where are the most intense thunderstorms on Earth? *Bull. Amer. Meteor. Soc.*, **87**, 1057–1071.